

CONFIDENTIAL

Copy 5
RM L57F17

C2

NACA RM L57F17



RESEARCH MEMORANDUM

INVESTIGATION OF THE LOW-SPEED PERFORMANCE AND
STATIC LONGITUDINAL STABILITY AND CONTROL CHARACTERISTICS
OF A 60° DELTA-WING-BODY-TAIL COMBINATION WITH BLOWING
OVER TRAILING-EDGE FLAPS

By William I. Scallion and Michael D. Cannon

CLASSIFICATION CHANGED

Langley Aeronautical Laboratory

UNCLASSIFIED Langley Field, Va.

To _____

LIBRARY COPY

By authority of *NASA TPA 9* *Effective*
9-1-59

AUG 1 1957

NB 11-23-59

CLASSIFIED DOCUMENT

LANGLEY AERONAUTICAL LABORATORY
LIBRARY, NACA

This material contains information affecting the National Defense of the United States within the meaning of the espionage laws, Title 18, U.S.C., Secs. 793 and 794, the transmission or revelation of which in any manner to an unauthorized person is prohibited by law.

NATIONAL ADVISORY COMMITTEE FOR AERONAUTICS

WASHINGTON

July 29, 1957

CONFIDENTIAL



NATIONAL ADVISORY COMMITTEE FOR AERONAUTICS

RESEARCH MEMORANDUM

INVESTIGATION OF THE LOW-SPEED PERFORMANCE AND
STATIC LONGITUDINAL STABILITY AND CONTROL CHARACTERISTICS
OF A 60° DELTA-WING—BODY—TAIL COMBINATION WITH BLOWING
OVER TRAILING-EDGE FLAPS

By William I. Scallion and Michael D. Cannon

SUMMARY

An investigation was made in the Langley full-scale tunnel to determine the effects of boundary-layer control by blowing over trailing-edge flaps on the low-speed performance and static longitudinal stability characteristics of a 60° delta-wing—body—tail combination incorporating variable flap positioning and leading-edge devices. The test Reynolds number was approximately 2.8×10^6 and the Mach number was 0.12.

Increasing the gap between the flap nose and the wing had a large effect on the minimum blowing required to achieve unseparated flow on the flap; however, with the gap sealed, the blowing requirements were not appreciably affected by moderate variations in vertical-flap position with respect to the blowing jet. The lift increments produced by blowing over semispan flaps were close to calculated theoretical values. Leading-edge separation reduced the lift increments produced by flap deflection and boundary-layer control; however, with full-span leading-edge devices the lift increments were maintained to maximum lift.

With boundary-layer control and a fixed horizontal tail, satisfactory longitudinal stability was obtained only with the tail located below the wing chord plane. The longitudinal stability of the model with high tail locations was improved by free floating the tail; however, the spanwise variation of downwash across the tail caused nonlinear characteristics.

The data indicate that significant reductions can be made in landing attitudes and approach speeds on delta-wing aircraft using boundary-layer control and a horizontal tail for trim.

CONFIDENTIAL

INTRODUCTION

Significant gains in low-speed performance of swept-wing airplanes have been indicated by the application of boundary-layer control by blowing over trailing-edge flaps (refs. 1 and 2). The realization of large lift increases obtainable with boundary-layer control, however, requires great care in the treatment of leading-edge stall control and in providing for a suitable horizontal-tail design for acceptable longitudinal stability and trim.

The boundary-layer-control research program in the Langley full-scale tunnel has been extended to include a 60° delta-wing—tail configuration. The purposes of this investigation were to determine the gains in low-speed performance made possible by a blowing flap and to what extent a rearward-located tail could be utilized on such a configuration. In view of the longitudinal instability known to exist for certain rearward fixed-tail locations on low-aspect-ratio wing configurations (for example, see refs. 3 and 4), it was reasoned that one possible solution to this problem would be to utilize a free-floating tab-controlled tail which would tend to reduce the effect of variation of downwash angle with angle of attack on the tail.

Aerodynamic forces and moments were obtained in the angle-of-attack range of -0.3° through the angle for maximum lift. The test Reynolds number was 2.8×10^6 and the Mach number was 0.12.

COEFFICIENTS AND SYMBOLS

Figure 1 shows the system of axes used and the positive direction of forces, moment, and angular displacement.

C_L	lift coefficient, $\frac{\text{Lift}}{q_\infty S}$
ΔC_L	increment of lift coefficient due to flap deflection and blowing over the flaps
C_D	drag coefficient, $\frac{\text{Drag}}{q_\infty S}$
C_m	pitching-moment coefficient, $\frac{\text{Pitching moment}}{q_\infty S \bar{c}}$

$\frac{dC_m}{dC_L}$	rate of change of pitching-moment coefficient with respect to lift coefficient at $C_L = 0$
c	wing chord, parallel to plane of symmetry, ft
\bar{c}	mean aerodynamic chord, $\frac{2}{S} \int_0^{b/2} c^2 dy$, ft
b	wing span, ft
S	wing area, sq ft
x	longitudinal distance from model pitch center to pivot of horizontal tail, ft
x'	longitudinal distance from nose of model, in.
z	distance along vertical axis, measured from model center line, ft
A	aspect ratio
C_μ	momentum coefficient, $\frac{w/gV_j}{q_\infty S}$
w	weight rate of flow, lb/sec
g	acceleration of gravity, 32.2 ft/sec ²
V_j	jet velocity assuming isentropic expansion, $\sqrt{\frac{2\gamma}{\gamma-1} RT \left[1 - \left(\frac{p_\infty}{p_t} \right)^{\gamma-1/\gamma} \right]}$, ft/sec
q_∞	free-stream dynamic pressure, $\frac{\rho_\infty V_\infty^2}{2}$, lb/sq ft
ρ_∞	mass density of free-stream air, slugs/cu ft
V_∞	free-stream velocity, ft/sec
V	velocity, knots
p	local static pressure, lb/sq ft

p_{∞}	free-stream static pressure, lb/sq ft
p_t	total pressure in wing duct, lb/sq ft
R	gas constant for air, $1,716 \frac{\text{ft-lb}}{\text{slug-}^{\circ}\text{R}}$
T	temperature in wing duct, $^{\circ}\text{R}$
γ	ratio of specific heats, 1.4 for air
α	angle of attack of wing chord line, deg
δ_f	angle of flap deflection with respect to wing chord line, deg
i_t	horizontal tail incidence angle with respect to wing chord line, deg
L/D	lift-drag ratio
W	airplane gross weight, lb
r	radius, in.

MODEL AND TESTS

The model used in this investigation had a 60° delta plan-form wing mounted symmetrically on a fuselage of circular cross section of fineness ratio 10. The wing had an aspect ratio of 2.31 and NACA 65A006 airfoil sections parallel to the plane of symmetry. A wing thickness of 6 percent was chosen as a minimum thickness consistent with the model size that would allow for sufficient internal ducting and a mechanically feasible adjustable slot for ejecting air over the flaps. Figure 2 presents a general layout of the model with pertinent dimensions and a list of the fuselage coordinates. A photograph of the model is presented in figure 3.

The model was equipped with plain trailing-edge controls having an approximately constant nose radius and hinged at approximately the 88-percent wing-root-chord position. Figure 2 shows the flap divided into two segments at the 0.56 semispan station; the inboard segment was designated as the semispan flap and the outboard segment was a horn-balance aileron. Both segments deflected alike constituted a full-span flap. The use of a horn-balance aileron prevented a longer span blowing slot as seen in figure 2. An adjustable flap hinge provided various vertical and horizontal positions relative to the blowing-jet center line and the flap nose, as shown in figure 4.

Air supply for the boundary-layer-control (BLC) system originated from an external source and was ducted to the flaps through the model support strut. This strut divided into a Y at the top with two outboard-opposing right-angle ducts, each supplying a separate wing panel. The model was attached to a strain-gage balance which was supported between the Y-shaped section of the strut. Flat circular labyrinth seals at the juncture of the wing panels and the Y-shaped section isolated the wing panels from the fixed supply ducts. The boundary-layer-control air was discharged over the flap from a slot located as shown in figure 4. The slot construction incorporated a series of adjusting screws by means of which the slot gap could be varied over a range from 0 to approximately 0.030 inch.

Two separate leading-edge configurations (fig. 5) were provided for investigation on the model during the test program and were designated leading edge A and B, respectively. Leading edge A was a leading-edge extension device with an approximate constant chord and it was twisted along the span. Leading-edge B was an extended leading-edge device with a tapered chord and a constant droop along the span.

Figure 6 shows the two horizontal-tail plan forms that were tested on the model. The area of each tail was 20 percent of the total wing area and the aspect ratios were 2.31 and 3.00, respectively, for the delta and unswept tails. They were mounted on an adjustable vertical strut allowing variation of position horizontally and vertically. Both tails were pivoted on a shaft so they could be used in either a fixed or floating condition. Each configuration was tested independently of the model to determine the floating characteristics about the chosen pivot point. The delta tail was found to be unstable at high tail angles of attack, and a permanent center tab with zero deflection was attached to the trailing edge in order to improve the floating characteristics. (See fig. 6.)

The model was tested through an angle-of-attack range of -0.3° to 34.8° at zero yaw for various flap deflections and leading-edge stall-control devices. A few tests were made with a full-span flap configuration, but the bulk of the testing was as a semispan configuration with the ailerons neutral. For the boundary-layer-control tests the values of blowing momentum coefficient ranged from 0 to 0.14 and the corresponding pressure ratios p_t/p_∞ were 0 to approximately 3.63. Tests were made with the horizontal tail at six different locations, as shown in figure 2, for $i_t = 0^\circ$ with and without flap deflection and boundary-layer control. Tests were also made for tail deflection angles of 0° , -15° , and -30° at the low rearward tail location. The delta tail and the unswept tail were tested free floating at the high forward location with several trailing-edge trim-tab deflections. The delta tail was deflected by using two outboard preset tabs as shown in figure 6, and an alternate center tab was also used. The center tab was of the same size as the permanent

stabilizing tab and it was attached in the same location, and this formed a split tab. (See inset A, fig. 6.) The unswept tail was deflected by a single preset center tab. All testing was conducted at a Reynolds number of approximately 2.8×10^6 based on the wing mean aerodynamic chord and the Mach number was about 0.12.

Aerodynamic forces and moments were obtained by use of a six-component internally mounted strain-gage balance system. The weight-rate flow delivered to the boundary-layer-control system was measured by an orifice meter installed in the supply line, and temperatures and pressures for slot-flow calculations were measured by thermocouples and shielded total pressure tubes, respectively, in the wing plenum chamber.

Computations were made for jet boundary (ref. 5) and buoyancy corrections, but were found to be negligible and were not applied.

A correction for stream misalignment of -0.3° was applied to the data. The drag data were corrected to compensate for obtaining the blowing air from an external source by adding an increment equal to $\frac{w/gV_\infty}{q_\infty S}$.

RESULTS AND DISCUSSION

Flap Lift Characteristics at Zero Angle of Attack

Effect of flap position, nose gap, and slot configuration.- The results of preliminary studies made with the full-span-flap configuration to determine an optimum flap-slot relationship for use in the remainder of the test program are summarized in figure 7(a). These results indicate that the effects of flap position in relation to the blowing jet are greatest in the low C_μ range where reattachment of the flap boundary layer is involved. An appreciable variation in minimum C_μ for flow reattachment (indicated by the portion of the curve for which the rate of increase of ΔC_L with C_μ markedly decreases) occurred for moderate variations in flap position and a very large effect is shown for the extremely low position with the nose gap unsealed. For the more normal positions (positions 1, 2, and 3) where the flap contour is approximately tangent to the jet center line or the wing contour, the variation in size of the nose gap appears to be the predominant factor reflected in the C_μ required for flow reattachment. The blowing jet tended to induce air flow through the gap and higher blowing-jet energy was required to overcome the mixing losses associated with the induced air flow. This is substantiated by the data for the flap in the low position (position 4) which was ineffective with the nose gap open but with the nose gap sealed, it was as efficient as the position where the nose gap was closed (position 2).

Some limited tests were made with the blowing slot tapered from root to tip to produce a constant C_{μ} distribution based on local wing chords; however, these results (fig. 7(a)) indicated that the constant height slot which produced a jet distribution proportional to the constant chord flap was somewhat better. The remainder of the test program was conducted with a constant height slot with the flap set in a vertical position corresponding to position 3 moved forward so that the gap between flap nose and wing shroud was approximately 0.0011c.

Effect of blowing on flap effectiveness.- The results of tests to evaluate the effects of blowing on several flap configurations at $\alpha = 0$ for a range of flap deflections are presented in figures 7(b) and 7(c). These results are generally similar to those of other investigations (for example, ref. 1) in that for all flap configurations sizeable initial gains in lift coefficient ΔC_L are obtained with relatively small momentum coefficients. This initial high blowing-jet effectiveness is associated with elimination of flow separation on the flap by reenergizing the boundary layer. A reduced rate of increase in ΔC_L occurred with further increases in momentum coefficient beyond the point where flow reattached. This further increase in lift is attributed in part to an induced loading over the forward and outboard portions of the wing and partly to the component of jet momentum reacting in the lift direction.

Observation of wool tufts on the surfaces of the full-span flap configuration indicated that for the 45° or 60° deflections the horn balance had a large detrimental effect on the overall effectiveness of the flap and that the lift gains shown in figure 7(b) were not as high as might be obtained. The horn-balance tip (over which blowing was not applied) was stalled, and, in addition, the surface discontinuity created by the horn caused separation on a portion of the flap even with blowing applied. The results of later tests made with the horn balance removed (diamond symbols in fig. 7(b)) showed a marked improvement in the effectiveness of this configuration. The data for the semispan flap (fig. 7(c)) showed that the gains in C_L attained by blowing over the flap increased with flap deflection and the momentum coefficient required to attain flow attachment also increased. As an example, the lift increment due to blowing (ΔC_L with blowing minus ΔC_L at $C_{\mu} = 0$) on the 35° flap was about one-half that for the 60° flap and flow cleanup was attained with momentum-coefficient values of approximately 0.004 and 0.01, respectively. This would be expected considering the more deteriorated flow condition existing for the higher flap deflections.

Comparison with theory.- A comparison of the flap lift increment produced by blowing sufficient to reenergize the boundary layer on the flaps with the calculated lift increment due to flap deflection (calculated by theoretical method of ref. 6) is presented in figure 8. The calculated values were based on the theoretical values of the two-dimensional flap-effectiveness parameter $(\alpha_{\delta})_{C_L}$ obtained by replacing

the ratio of flap chord to wing chord with a ratio of flap area to wing exposed area. The symbol points in figure 8 correspond to the tick marks on the curves of figures 7(b) and 7(c). The experimental semispan-flap lift increments at the lower flap deflections agreed reasonably well with those predicted by the theory. The reduced effectiveness at the higher flap deflections is attributed to flow disturbances at the ends of the flap. The experimental lift increments produced by the full-span flaps with the horn tips (aspect ratio, 2.31) were much less than the theoretical increments, as would be expected from the observed flow interferences. With the horn tips removed (aspect ratio, 1.47), the experimental value was somewhat closer to that predicted by the theory.

Tail-Off Characteristics

Basic model, flaps neutral.- The longitudinal characteristics of the basic model are presented in figure 9. The basic model with plain leading edges attained a maximum lift coefficient of 1.12 at an angle of attack of 32° (fig. 9(a)) and the model was longitudinally stable to the stall. The addition of the full-span twisted leading-edge chord-extension (leading edge A) delayed the formation of the leading-edge separation vortex, increased the maximum lift coefficient to 1.33 at an angle of attack of 34.8° , and except at low lift coefficients reduced the drag for a given lift coefficient.

Semispan flaps deflected.- The longitudinal data obtained for the various flap deflections are presented in figures 10, 11, and 12. Examination of the data indicates that from consideration of drag and obtainable maximum lift the 35° and 45° flap deflections appear to be near the optimum for this wing configuration; however, the 45° flap appeared somewhat better from the standpoint of lift at a given angle of attack. The results for various flap deflections reflect similar trends and the following discussion will therefore concentrate on the data for the 45° flap deflection, since a greater range of configurations is available for this condition.

Deflection of the semispan flaps 45° produced a lift coefficient of 0.3 above that of the basic model at zero angle of attack (fig. 11(a)), and blowing over the flaps ($C_\mu = 0.017$) produced an additional lift increment of 0.2. At high values of α there was a decrease in lift-curve slope and the lift increment at maximum lift was considerably reduced. The decreased lift and rapid drag increase above lift coefficients of 0.8 are caused by leading-edge separation (refs. 1 and 7). Therefore, a leading-edge droop was incorporated to determine whether the lift increment could be maintained and the drag reduced at higher angles of attack. With the full-span constant-chord leading-edge device installed (leading edge A of fig. 5), the lift increment obtained by blowing over the flaps ($C_\mu = 0.017$) was almost constant throughout the angle-of-attack range and

produced a maximum lift coefficient (fig. 11) of 1.59 at $\alpha = 29.5^\circ$ with drag coefficients appreciably reduced.

Leading-edge device A was not considered ideal insofar as practical application was concerned (the leading edge was twisted along the span as shown in fig. 5) so a leading-edge device with a constant droop and tapering in chord along the span was installed (leading edge B). As can be seen, the maximum lift coefficient obtained for this configuration was somewhat lower (1.48); however, the angle of attack for maximum lift in either case is higher than would probably be considered usable and both the lift and drag coefficient obtained were about the same for either leading-edge device below angles of attack of 24° .

As was expected, deflection of the semispan flaps produced a large negative increment in pitching-moment coefficient. Blowing over the semispan flaps ($C_{\mu} = 0.017$) added a further negative increment in pitching-moment coefficient at approximately -0.10 through the lift-coefficient range.

A comparison of the data for identical configurations in figure 11(b) showed that at the higher lift coefficients blowing over the semispan flaps decreased the drag. This is due in part to the difference in configuration profile and parasite drag since the angle of attack of the model for a given lift coefficient with blowing over the flaps is about 8° less than that for the same configuration without blowing.

At low to moderate lift coefficients (between $C_L = 0.5$ and $C_L = 0.88$), blowing over the semispan flaps increased the drag coefficient. The effect of blowing over the flaps on drag at low lift coefficients (or where extensive wing separation has not occurred) is primarily dependent upon the span of the flap over which the blowing is applied and the flap deflection. The increase in drag on the model in this case (the data in fig. 11(b)) is associated with the increased effectiveness of the short semispan flap which produced a large distortion in the wing-span load distribution and, consequently, an increase in the induced drag. Data (not presented herein) for the model of this investigation showed that, at the lower lift coefficients, blowing (at the same momentum coefficient as on the semispan flaps) over the full-span flaps (deflected 45°) reduced the drag of the full-span-flap configuration. This is also shown in the data for the model of reference 1.

Tail-On Characteristics

Tail fixed.- The effects of horizontal-tail position on the longitudinal stability of the model with the flaps neutral, semispan flaps deflected 45° , and with blowing over the semispan flaps are shown in figure 13.

With the flaps neutral, the model was longitudinally stable through the complete lift-coefficient range for tail locations $0.25\bar{c}$ above and $0.14\bar{c}$ below the wing chord plane. (See figs. 13(a), (b), (d), and (e).) For the higher tail locations ($0.50\bar{c}$ above the wing chord plane), the model was unstable at the higher lift coefficients. (See figs. 13(c) and (f).)

Deflection of the semispan flaps 45° reduced the longitudinal stability of the model with the tails located above the wing chord plane (by increasing the wing downwash in the region of the tail) for lift coefficients above approximately 0.8. (See figs. 13(b), (c), (e), and (f).) Application of blowing over the deflected flaps further increased the downwash at the tail to the extent that the only satisfactory tail positions from the standpoint of longitudinal stability were those below the wing chord plane. (See figs. 13(a) and (d).)

The effects of horizontal-tail deflection on the longitudinal characteristics of the model with the tail located $0.14\bar{c}$ below the wing chord plane and $2.0\bar{c}$ behind the pitch center are shown in figure 14. The tail had adequate power to trim the model through the angle-of-attack range. (See fig. 14(a).) The static margin of this configuration was rather high, $dC_m/dC_L = 0.21$ (obtained from fig. 13(a) for the configuration with flaps neutral). As a result, there would be an appreciable loss in lift due to trim. The maximum trim lift coefficient of the model with this static margin was about 1.40; whereas, a reduction in the static margin to -0.075 (with the flaps neutral) would result in an increase in trimmed maximum lift coefficient to about 1.57. The obtainable landing lift coefficient of an airplane with the low and rearward tail, however, would depend upon the angle of attack near the ground (with adequate tail clearance) that might be obtained with this arrangement.

Tail free.- In an effort to obtain longitudinal stability on the model with the tail located above the wing chord plane, the delta tail was free-floated at a position $0.50\bar{c}$ above the wing chord plane and $1.5\bar{c}$ behind the pitch center. With this method the tail would be free to maintain an approximately constant attitude and loading with respect to the downwash, and the detrimental change in stability caused by the overpowering influence of the wing vortices and associated variation of downwash with angle of attack would be reduced. The results of these tests are shown in figures 15 to 17.

A comparison of the longitudinal stability of the model with the flaps neutral and with the tail fixed and tail free (fig. 15(a)) shows that longitudinal stability was attained for higher lift coefficients with the tail free; however, the model was unstable near maximum lift. This was also the case for the model with the flaps deflected and with blowing over the flaps (figs. 16(a) and 17(a)). An increase in stability occurs for all three cases (flaps neutral, deflected, and with blowing)

at a lift coefficient corresponding to an angle of attack of approximately 16° . This increase was quite abrupt (occurring within an angle-of-attack range of 1° to 2°) when the tabs were deflected for trim on the configurations with flaps deflected and with blowing applied. (See figs. 16(a) and 17(a)). A comparison of the tail-off and tail-free moment curves indicates that the free-floating tail experienced an increasing positive lift load (as shown by the negative increment in C_m for the free tail) at lift coefficients corresponding to angles of attack above 16° . As can be seen from the small plots in figures 15(a), 16(a), and 17(a), this positive increase in tail loading was apparently caused by a positive increase in tail floating angle i_t , between $\alpha = 16^\circ$ and $\alpha = 28^\circ$. This was indicative of a nonuniform spanwise distribution of the wing downwash and dynamic pressure across the tail. Flow studies with a long streamer in the region of the tail indicated that the inboard edges of the wing leading-edge separation vortices impinged on the tip sections of the tail. This produced a positive moment about the tail hinge line and, consequently, produced a positive tail angle of attack and lift relative to the downwash over the inboard portion of the tail. An accurate representation of the flow field behind a delta wing (with the flaps neutral), showing the location of the separation vortex in a plane located in the region of the floating tail of this investigation, is shown in figure 8 of reference 8. The differences in shape of the tail incidence curves with the tabs deflected as shown in figures 16(a) and 17(a) (with and without blowing on the deflected flaps) may be attributed to changes in the tail stability characteristics associated with the variation in tab configurations. Because of the aforementioned phenomena associated with the floating characteristics of the delta tail, the maximum trim lift coefficient that could be attained with the tail free and with blowing over the flaps was limited to approximately 1.08.

It was believed that a floating tail with a uniform area distribution about the pivot point might reduce the rather abrupt increase in stability, which results from spanwise variations of downwash angle over the delta tail. The results of tests with an unswept tail of the same area as the delta tail are shown in figure 18. It can be seen from this figure that the increase in longitudinal stability at high angles of attack was considerably smaller than that for the delta tail and a smoother variation of C_m with C_L was obtained; however, the maximum lift of the unswept tail was less than that of the delta tail and, therefore, the model could not be trimmed.

In view of the influence of the longitudinal characteristics of the tail itself and of the plan form of the tail on the degree of stability and trim that could be obtained on the model, further investigation of these factors would be necessary in order to evaluate more fully the characteristics of a delta-wing model with a free-floating tail.

Low-Speed Performance Characteristics

The variation of thrust required with velocity for a hypothetical delta-wing airplane with a gross weight of 30,000 pounds and a total wing area of 500 square feet is shown in figure 19 for several simulated-flight landing-approach configurations. All configurations utilized a tail for trim except for the configuration using trailing-edge flap controls. Tick marks are placed on the curves to indicate the airplane attitudes in increments of 4° . The boundary-layer-control curve was calculated for a constant blowing-air rate of 6 lb/sec, and the data were corrected for the variation of C_{μ} with velocity, so that the curve more nearly represents an actual flight curve. The value of C_{μ} representing completely unseparated flow on the flap would occur at about 134 knots ($C_{\mu} \approx 0.008$).

The use of flaps with or without boundary-layer-control has an appreciable effect on the thrust required in that the thrust required is much higher than that of the airplane with flaps neutral or the tailless airplane. The variation of thrust required with velocity was decreased on the flapped configuration when boundary-layer control was applied (between $\alpha = 0^\circ$ and 8°) and speed control might be difficult to achieve because of the relatively flat curve in this range; that is, small variations in thrust could result in large variations in speed.

The use of boundary-layer control produces much slower approach speeds for a given attitude. For example, if a 12° approach attitude for the configuration with boundary-layer control were assumed, an approach speed of approximately 130 knots would result; whereas, without boundary-layer control with a tail for trim and flaps deflected, a speed of approximately 155 knots is indicated. For the tailless airplane without flaps this same attitude would result in a speed of 209 knots. It is also of interest to note that for the boundary-layer-control configuration the aforementioned conditions ($\alpha = 12^\circ$, $V = 130$ knots) are reached without any appreciable increase in thrust requirements as speed reduces. However, all other configurations would increase attitude and fly well up the back side of the power curve to reach a comparable approach speed.

Although this limited type of analysis does not provide a definite evaluation of landing gains, it does indicate that for a delta-wing airplane with a horizontal tail considerable reductions in landing attitudes and approach speeds may be obtained with a suitably integrated blowing-flap system.

CONCLUSIONS

The results of a wind-tunnel investigation to determine the effects of boundary-layer control by blowing over trailing-edge flaps on the static

longitudinal stability characteristics of a 60° sweptback delta-wing—fuselage combination incorporating variable flap to blowing-jet relationships, leading-edge devices, and horizontal tails indicate the following conclusions:

1. Increasing the gap between the flap nose and the wing had a large effect on the minimum blowing required to achieve unseparated flow on the flap; whereas, blowing requirements with the gap sealed, were not appreciably affected by moderate variations in vertical positioning of the flap with respect to the blowing jet.

2. Blowing over the semispan flaps produced lift increments close to calculated values; however, lift increments with full-span flaps were considerably less due to the stalled horn-balance flow disturbance on adjacent outboard flap segments. Removal of the horn balance restored lift increments close to the calculated values.

3. Leading-edge devices preserved lift gains from boundary-layer control throughout the angle-of-attack range and produced appreciable drag reduction throughout most of the lift-coefficient range.

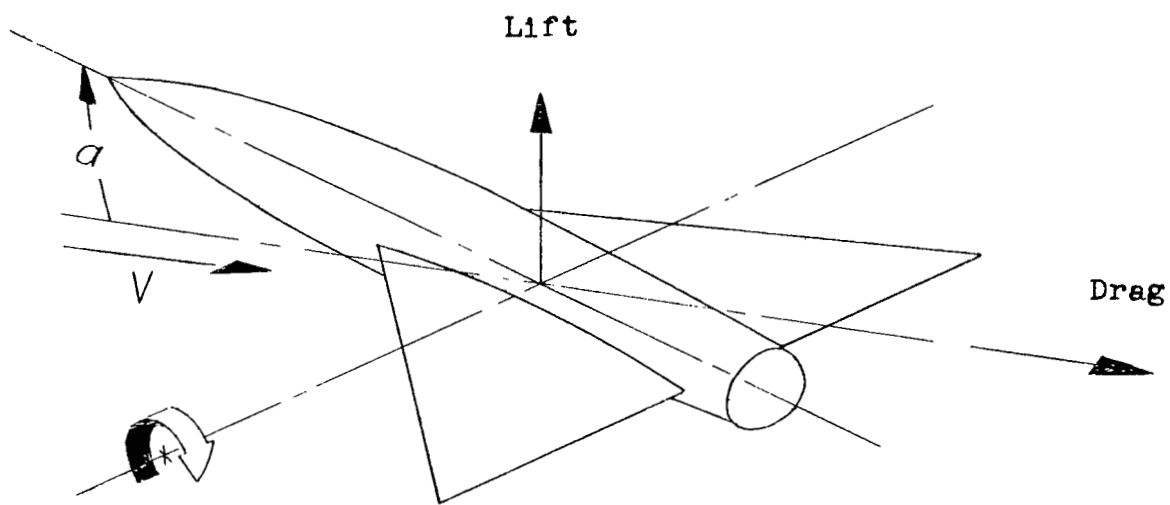
4. With boundary-layer control applied to the flaps, the only satisfactory fixed-tail positions from the longitudinal stability standpoint were those below the wing chord plane. Stability characteristics for high tail locations were somewhat improved by free floating the tail, but linear characteristics could not be obtained due to effects of spanwise variation in downwash at the tail. The plan form of the tail greatly influenced the degree of stability and trim that could be obtained on the model.

5. Calculations for a hypothetical delta-wing aircraft based on the data of this report indicate that it is possible to obtain marked reductions in landing attitude and approach speeds by using boundary-layer control and a horizontal tail for trim.

Langley Aeronautical Laboratory,
National Advisory Committee for Aeronautics,
Langley Field, Va., June 3, 1957.

REFERENCES

1. McLemore, H. Clyde, and Fink, Marvin P.: Blowing Over the Flaps and Wing Leading Edge of a Thin 49° Swept Wing-Body-Tail Configuration in Combination With Leading-Edge Devices. NACA RM L56E16, 1956.
2. Kelly, Mark W., and Tolhurst, William H., Jr.: Full-Scale Wind-Tunnel Tests of a 35° Sweptback Wing Airplane With High-Velocity Blowing Over the Trailing-Edge Flaps. NACA RM A55I09, 1955.
3. Jaquet, Byron M.: Effects of Horizontal-Tail Position, Area, and Aspect Ratio on Low-Speed Static Longitudinal Stability and Control Characteristics of a 60° Triangular-Wing Model Having Various Triangular-All-Movable Horizontal Tails. NACA RM L51I06, 1951.
4. Riebe, John M., and Graven, Jean C., Jr.: Low-Speed Investigation of the Effects of Location of a Delta Horizontal Tail on the Longitudinal Stability and Control of a Fuselage and Thin Delta Wing With Double Slotted Flaps Including the Effects of a Ground Board. NACA RM L53H19a, 1953.
5. Katzoff, S., and Hannah, Margery E.: Calculation of Tunnel-Induced Upwash Velocities for Swept and Yawed Wings. NACA TN 1748, 1948.
6. Lowry, John G., and Polhamus, Edward C.: A Method for Predicting Lift Increments Due to Flap Deflection at Low Angles of Attack in Incompressible Flow. NACA TN 3911, 1947.
7. Pocock, P. J., and Westell, J. R.: The Induced Drag Factor of Highly Swept Delta Wings at Subsonic Speeds. Lab Memo. AE-6b, Nat. Aero. Establishment (Ottawa), Apr. 22, 1952.
8. Whittle, Edward F., Jr., and Hawes, John G.: Investigation at Low Speed of the Downwash, Sidewash, and Wake Characteristics Behind a Large-Scale Triangular Wing, Including the Effects of Yaw, Full-Span Trailing-Edge Flaps, and Two Leading-Edge Modifications. NACA RM L52H19, 1952.



Pitching moment

Figure 1.- System of axes used. Arrows indicate positive direction of forces, moment, and angular displacement.

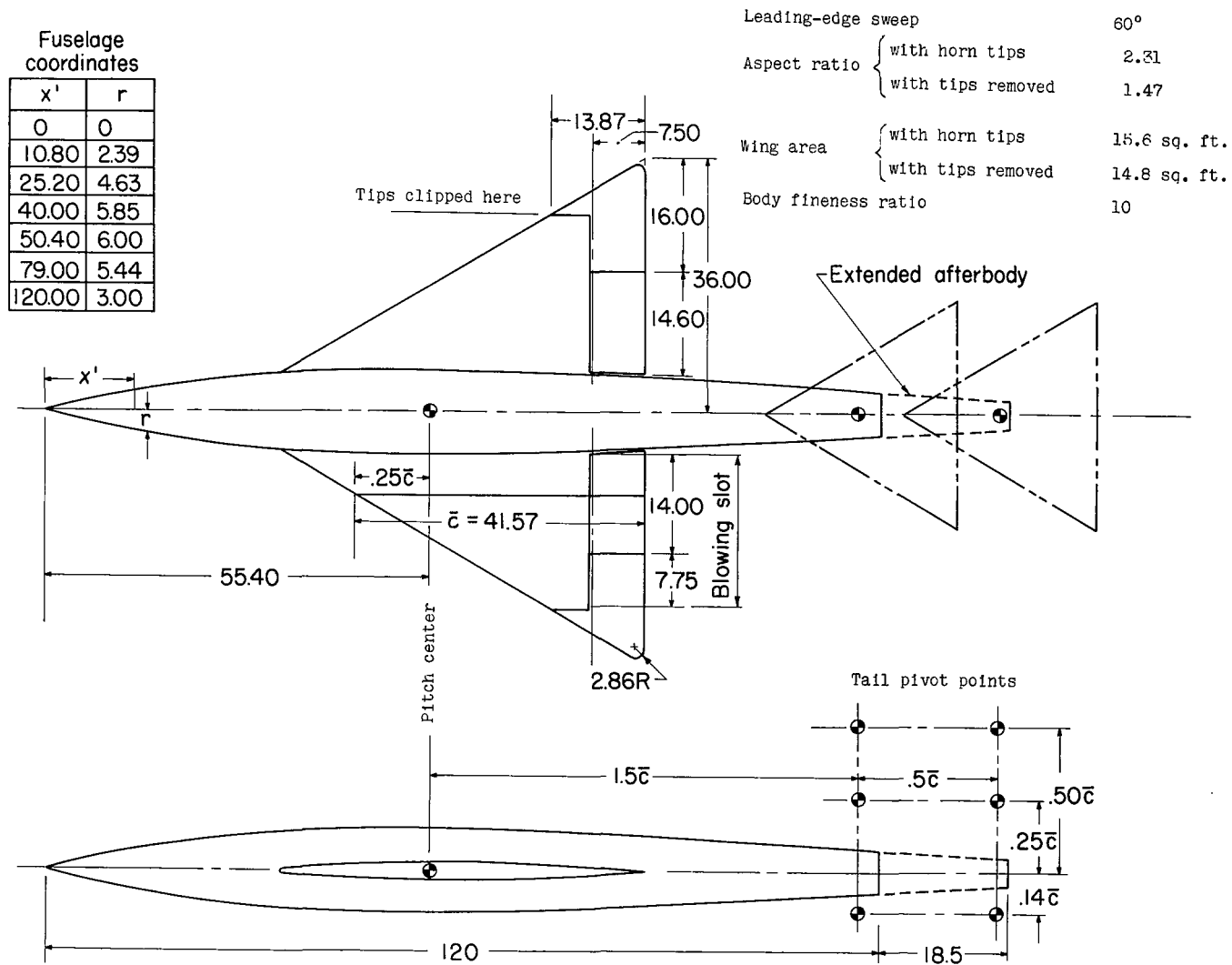


Figure 2.- General arrangement and principal dimensions of the 60° delta-wing model. (Dimensions are in inches.)

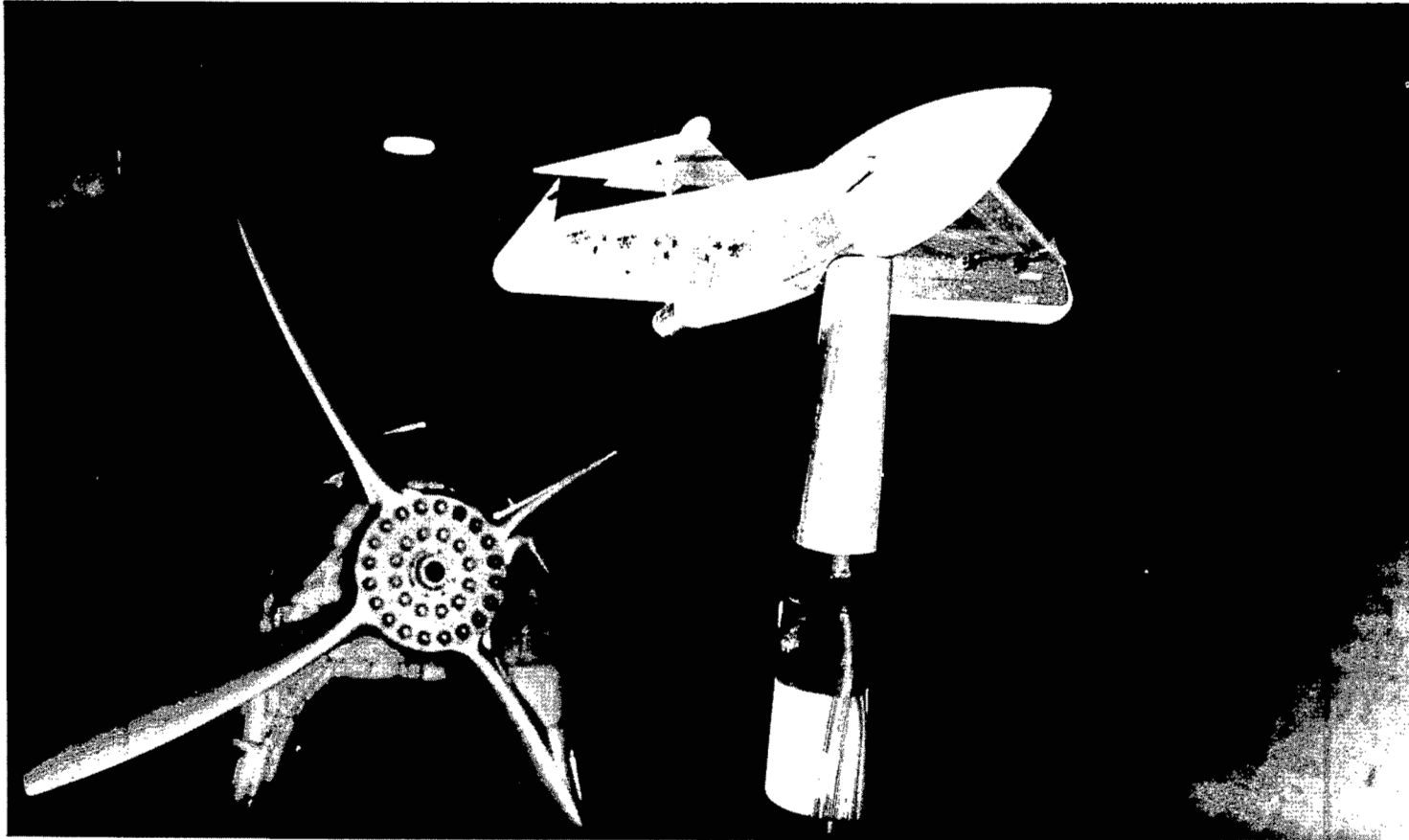


Figure 3.- Photograph of the delta-wing model in the Langley full-scale tunnel. L-92256

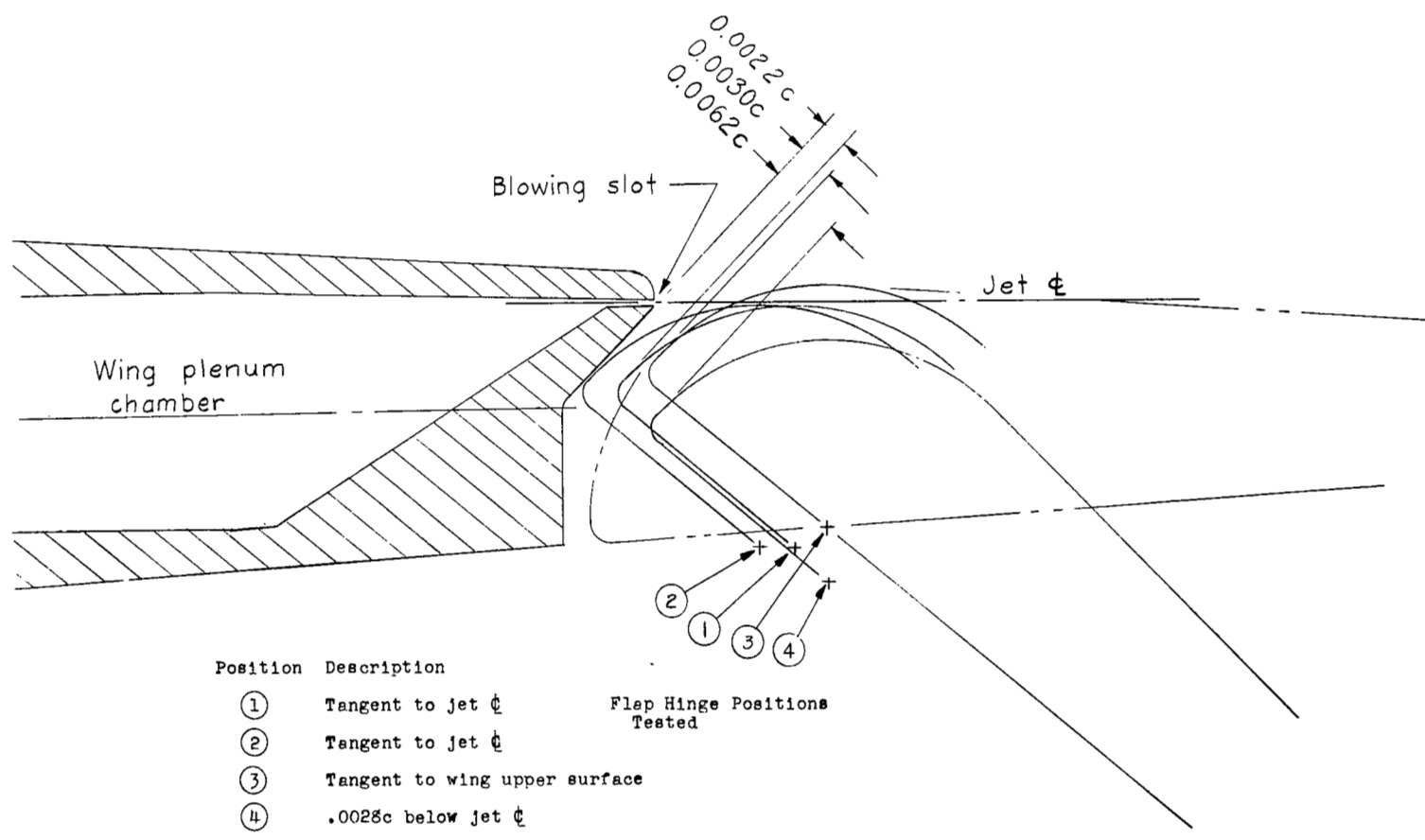


Figure 4.- Details of the trailing-edge blowing slot and flap positions at the inboard end of the flap.

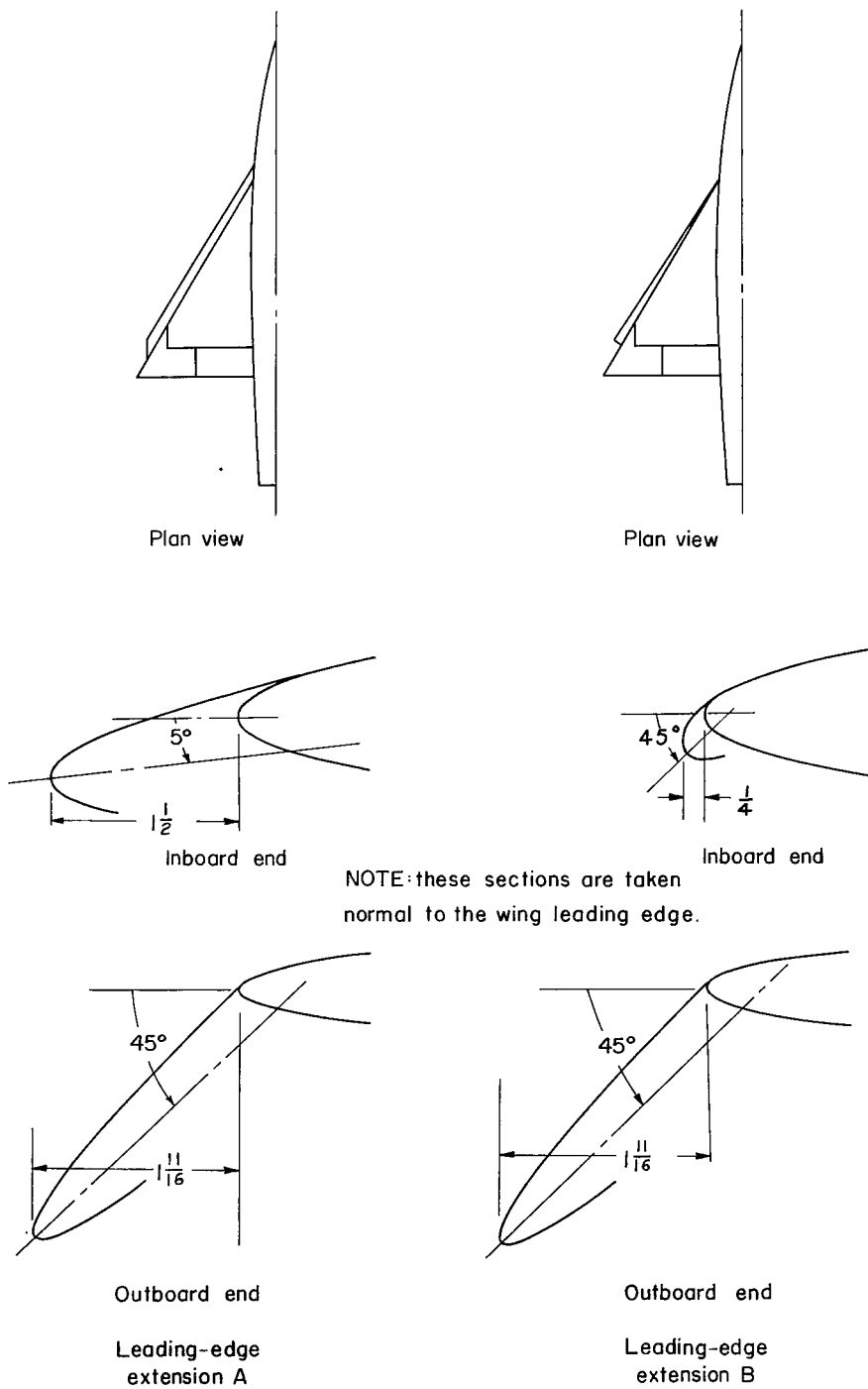
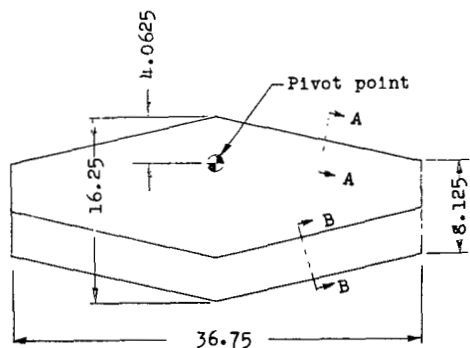
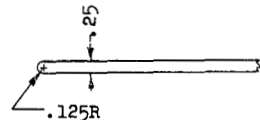


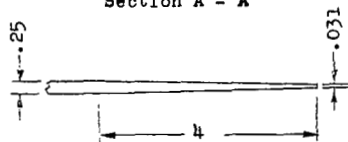
Figure 5.- Sketches of the leading-edge devices. (Dimensions are given in inches.)



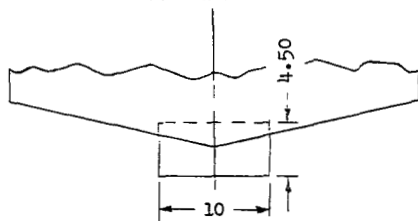
Plan View



Section A - A

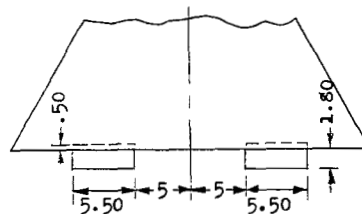


Section B - B

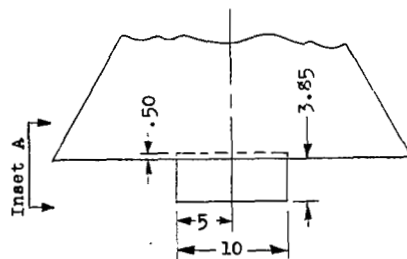


Center tab - Unswept tail

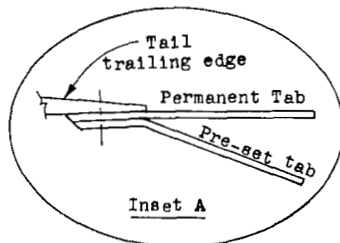
UNSWEPT TAIL



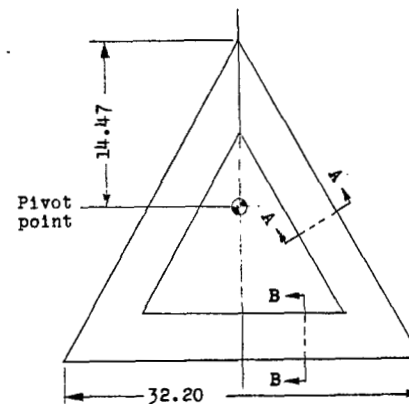
Outboard tabs - Delta tail



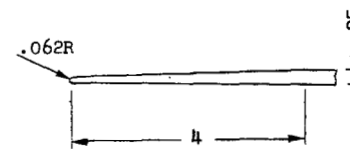
Center tab - Delta tail



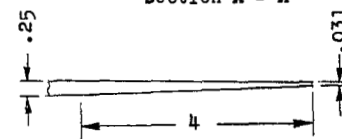
Inset A



Plan View



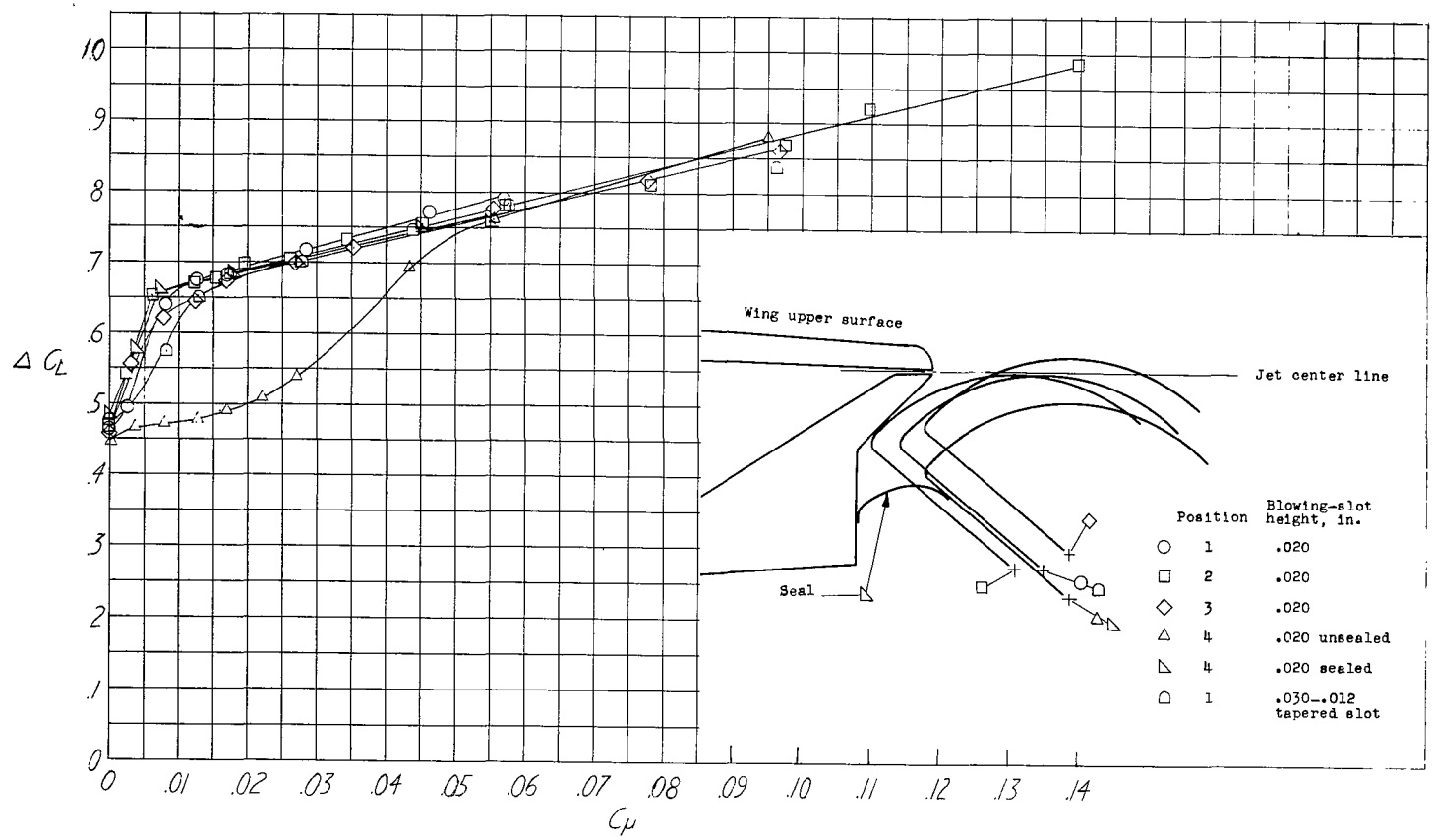
Section A - A



Section B - B

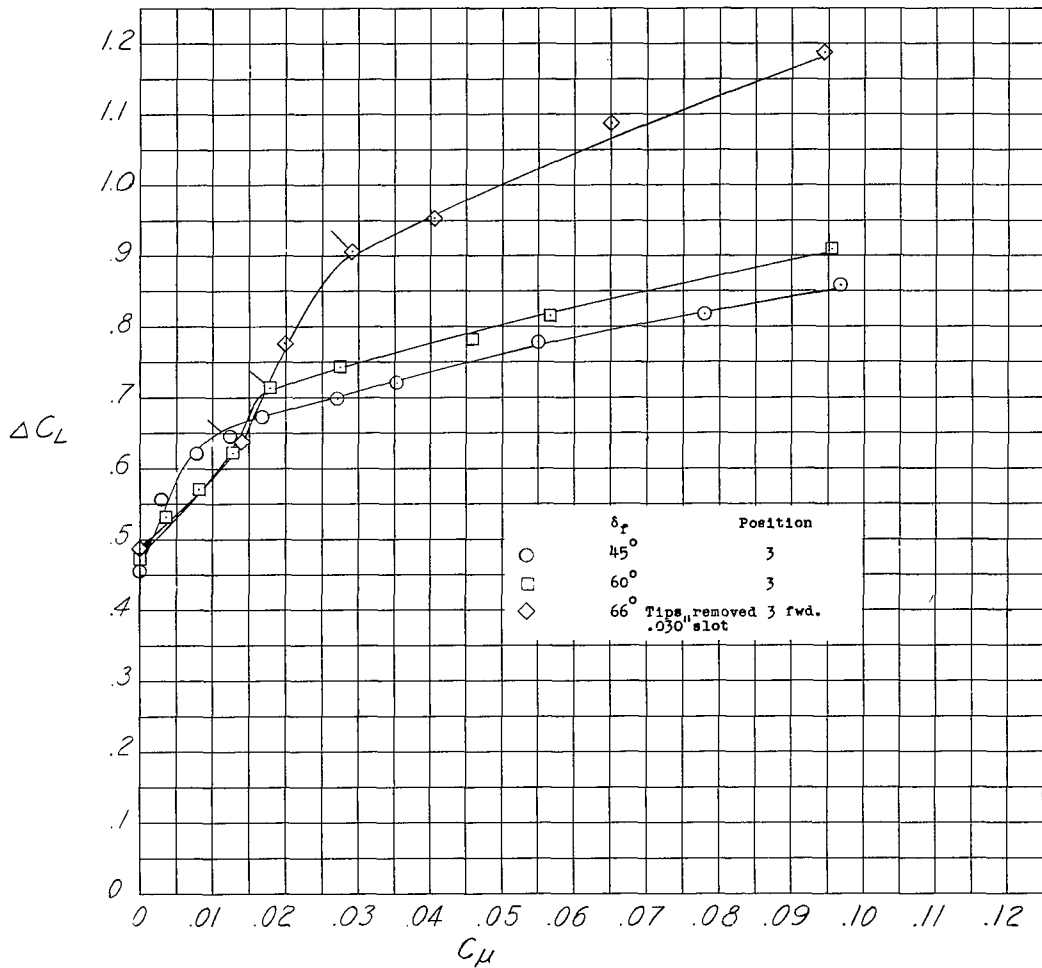
DELTA TAIL

Figure 6.- Sketches of delta and unswept tail with trim-tab arrangements. (Dimensions are given in inches.)



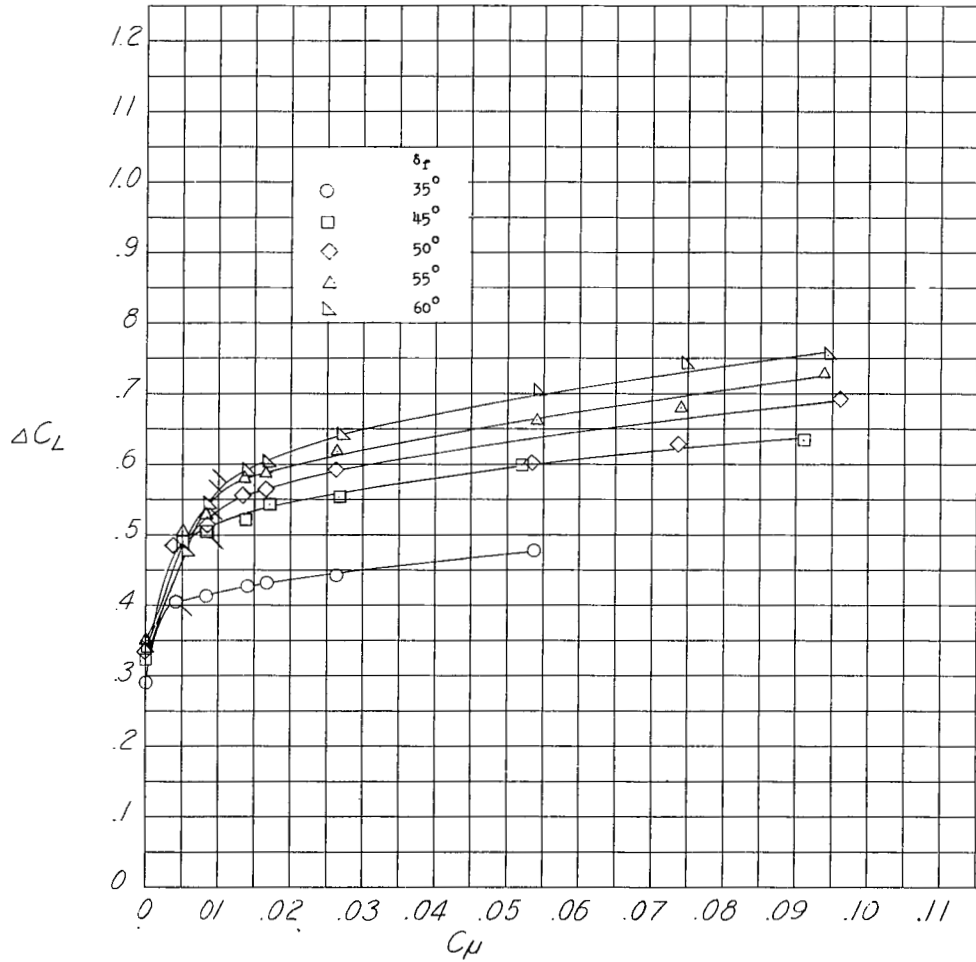
(a) Effects of position, full-span flaps, $\delta_f = 45^\circ$.

Figure 7.- Variations of ΔC_L with C_μ at zero angle of attack.



(b) Full-span flaps.

Figure 7.- Continued.



(c) Semispan flaps, position 3 forward.

Figure 7.- Concluded.

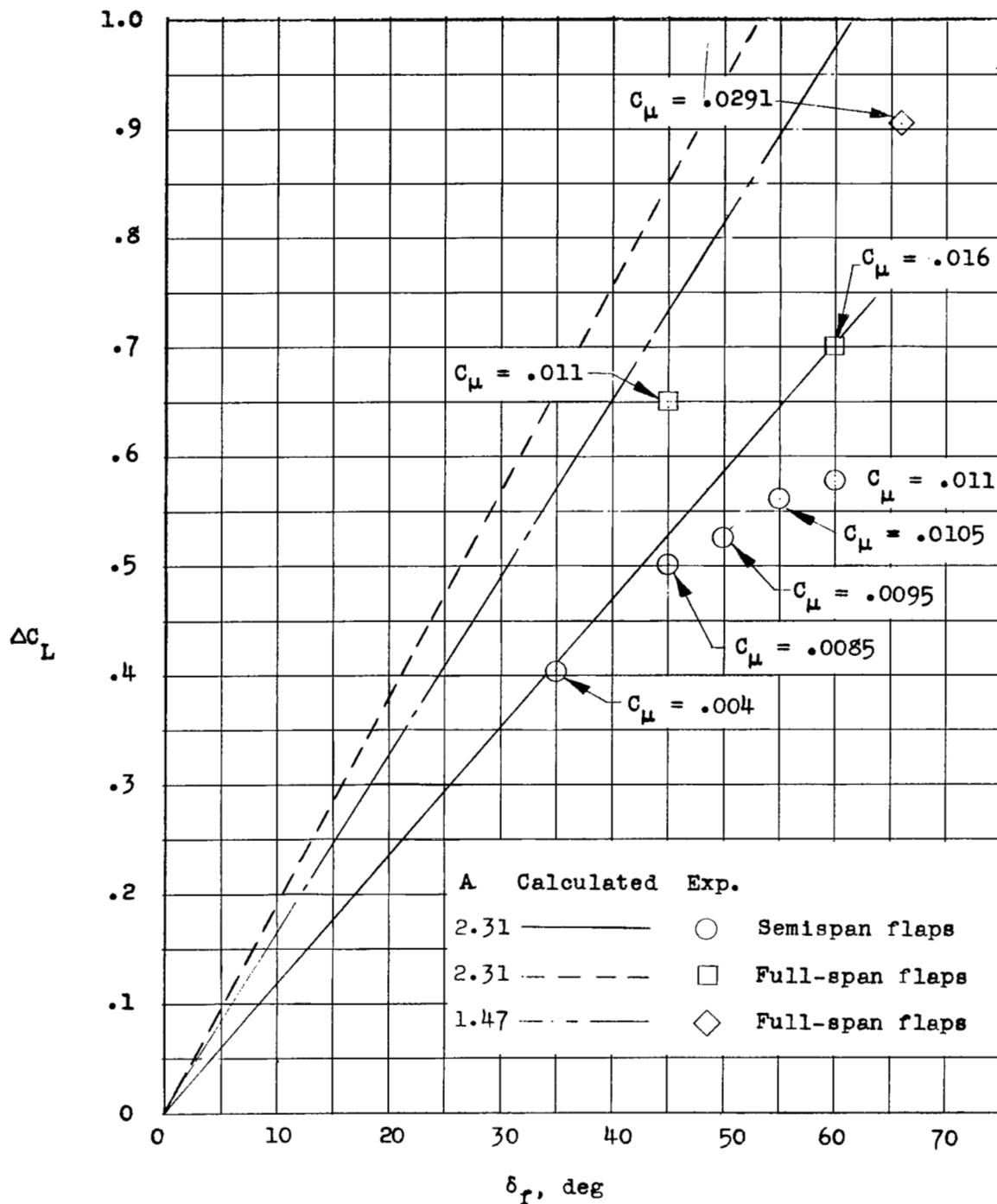
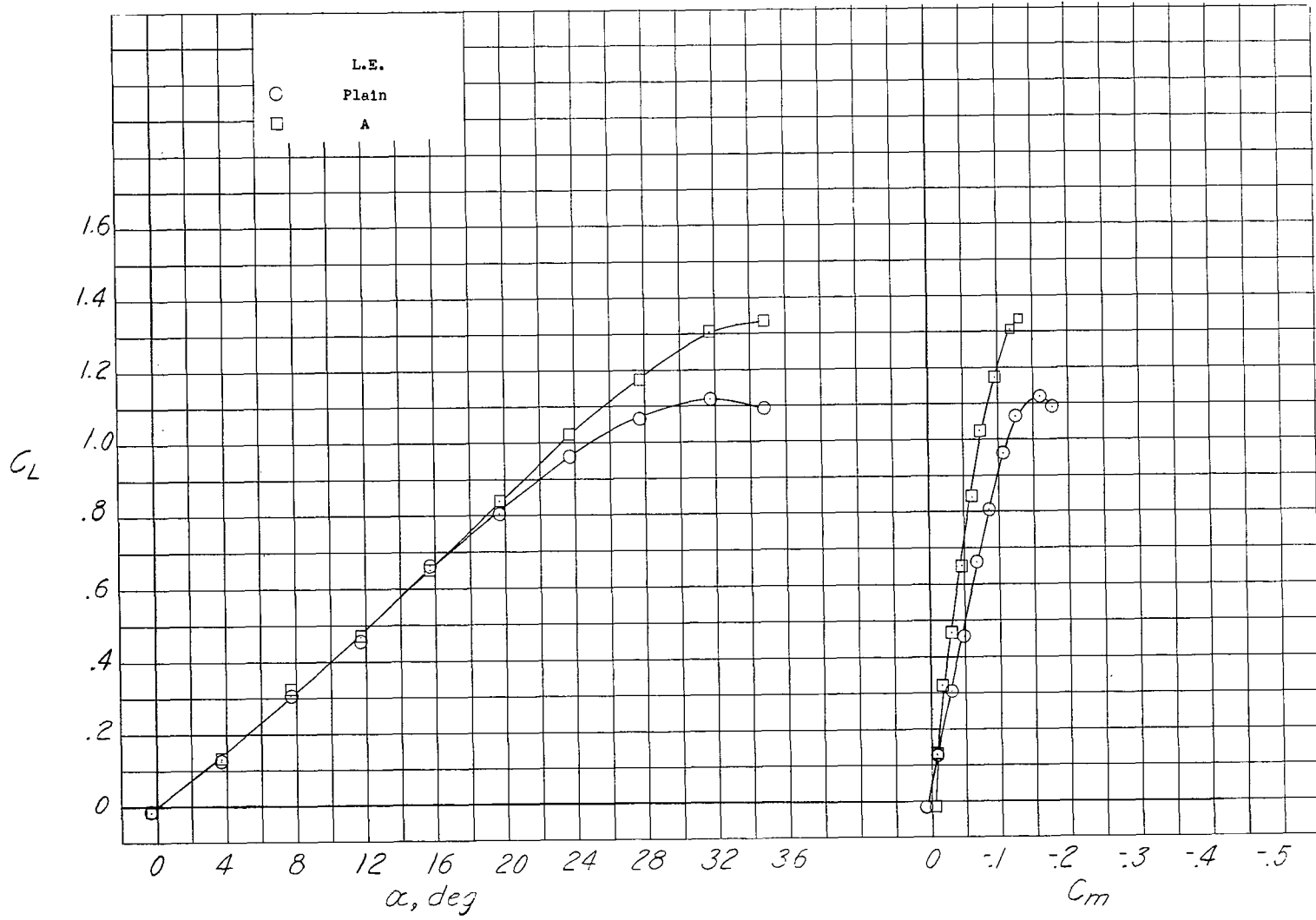
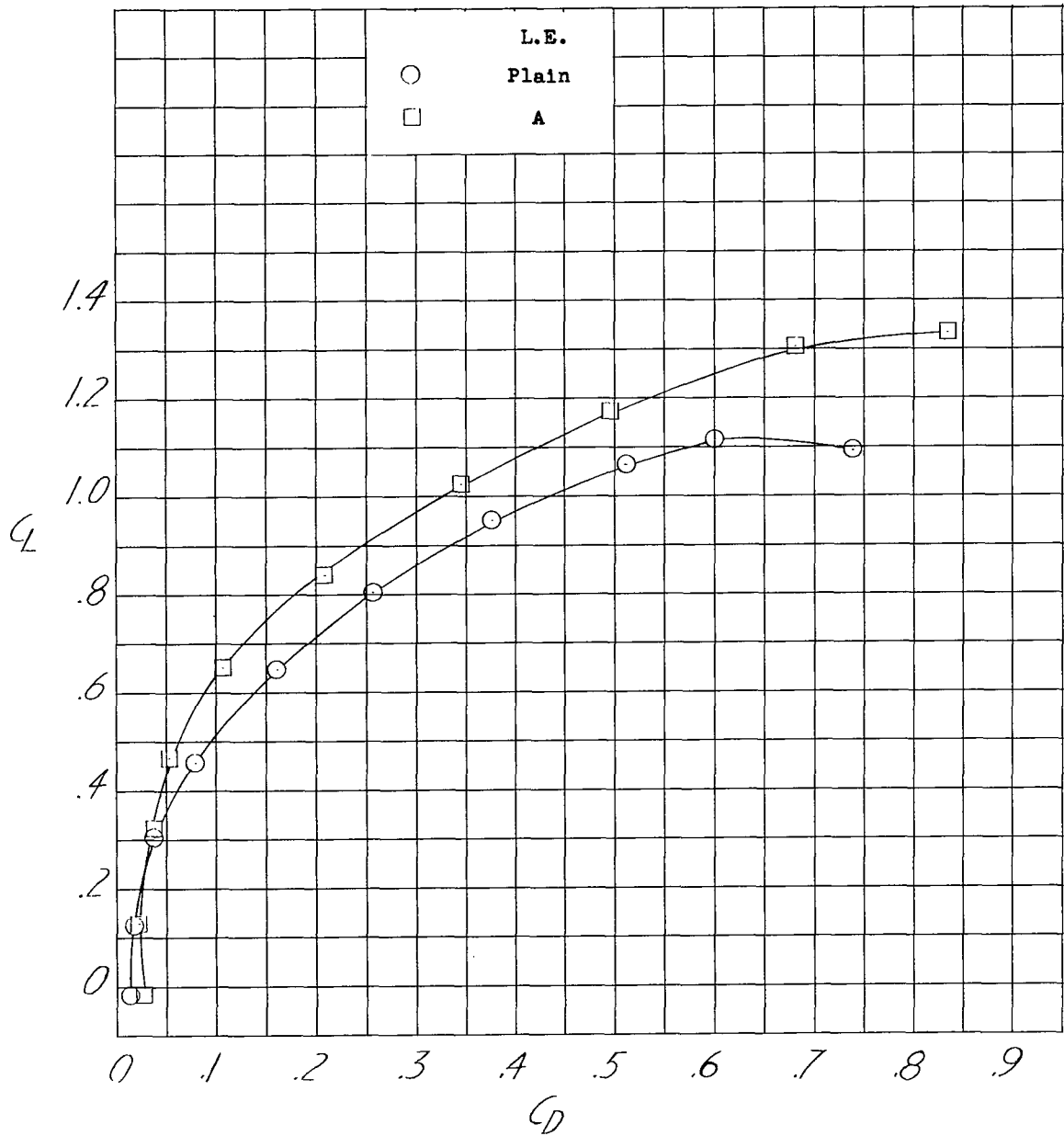


Figure 8.- Comparison of the theoretical flap effectiveness with that obtained experimentally. $\alpha = 0^\circ$.



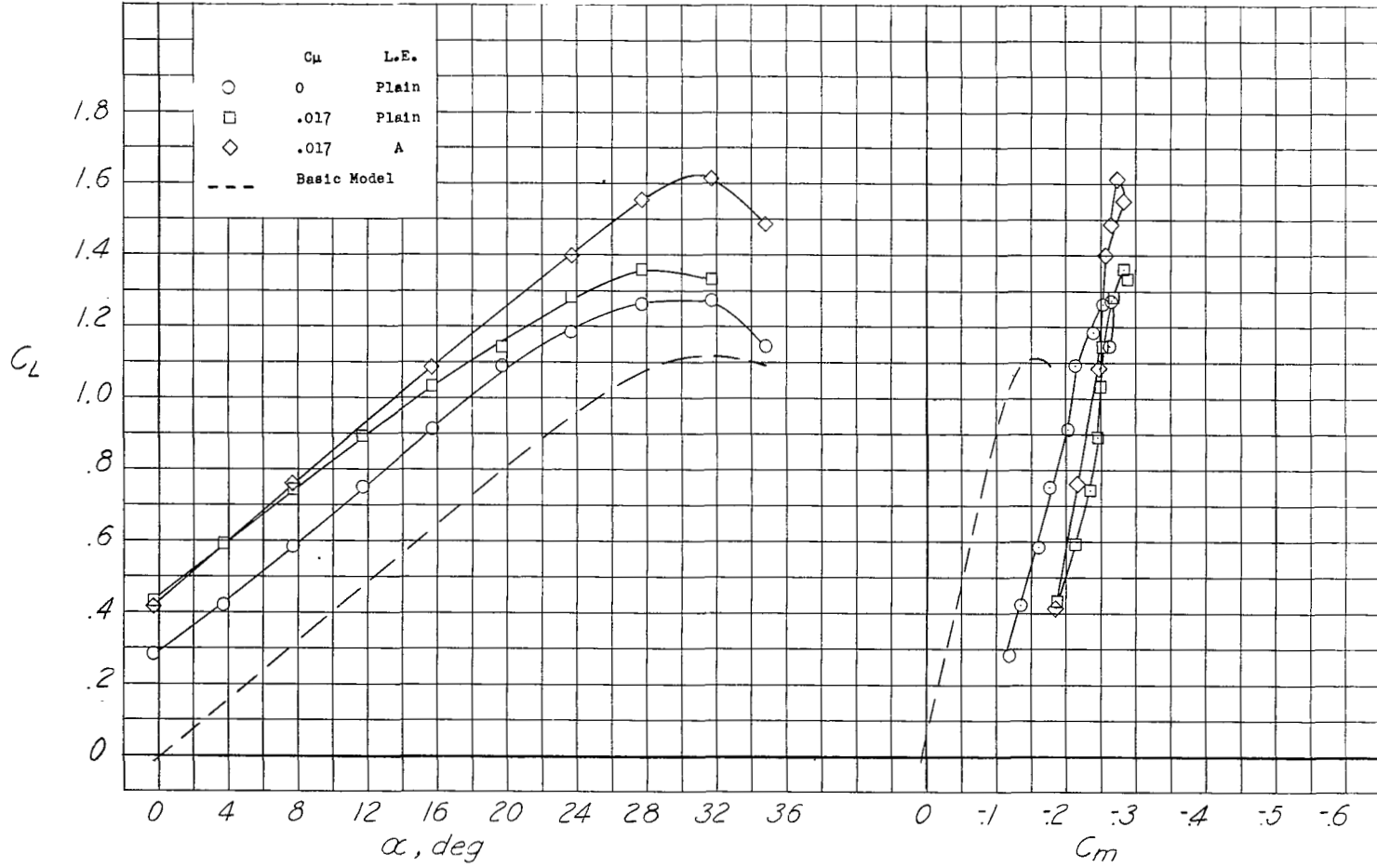
(a) Lift and pitching moment.

Figure 9.- Longitudinal characteristics of the basic model. Tail off; $\delta_f = 0^\circ$.



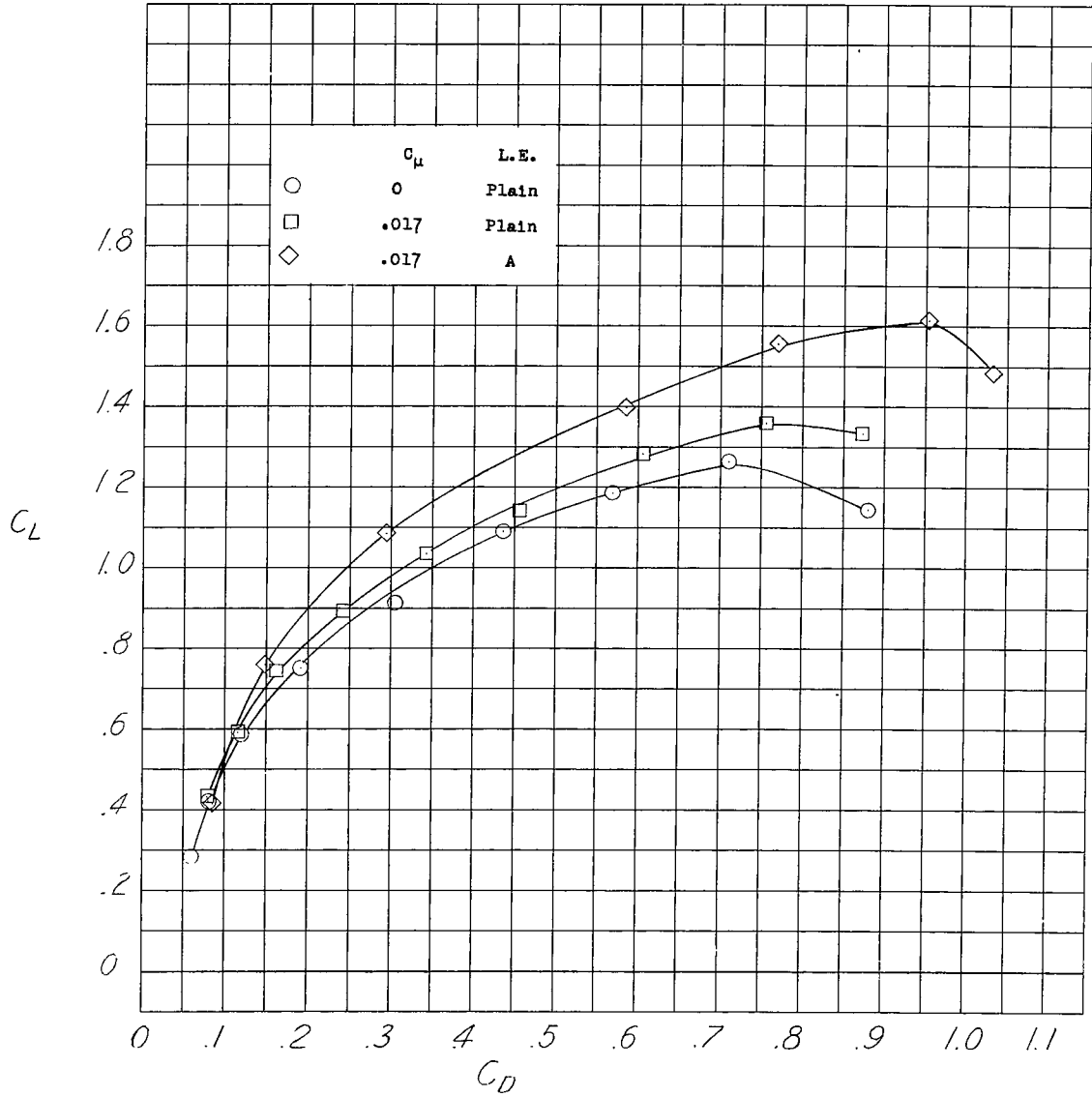
(b) Drag.

Figure 9.- Concluded.



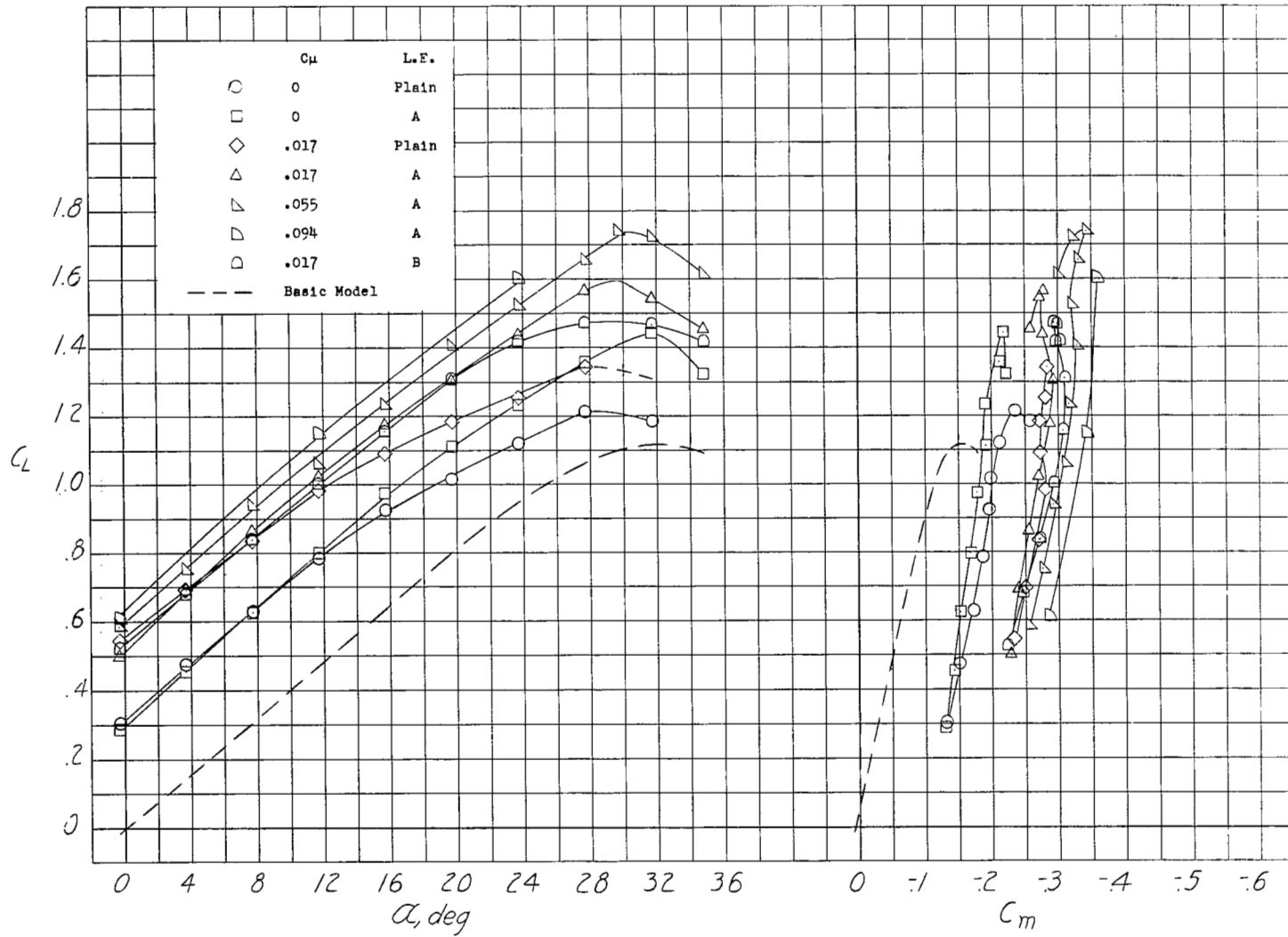
(a) Lift and pitching moment.

Figure 10.- Longitudinal characteristics of the model with semispan flaps deflected 35°. Tail off.



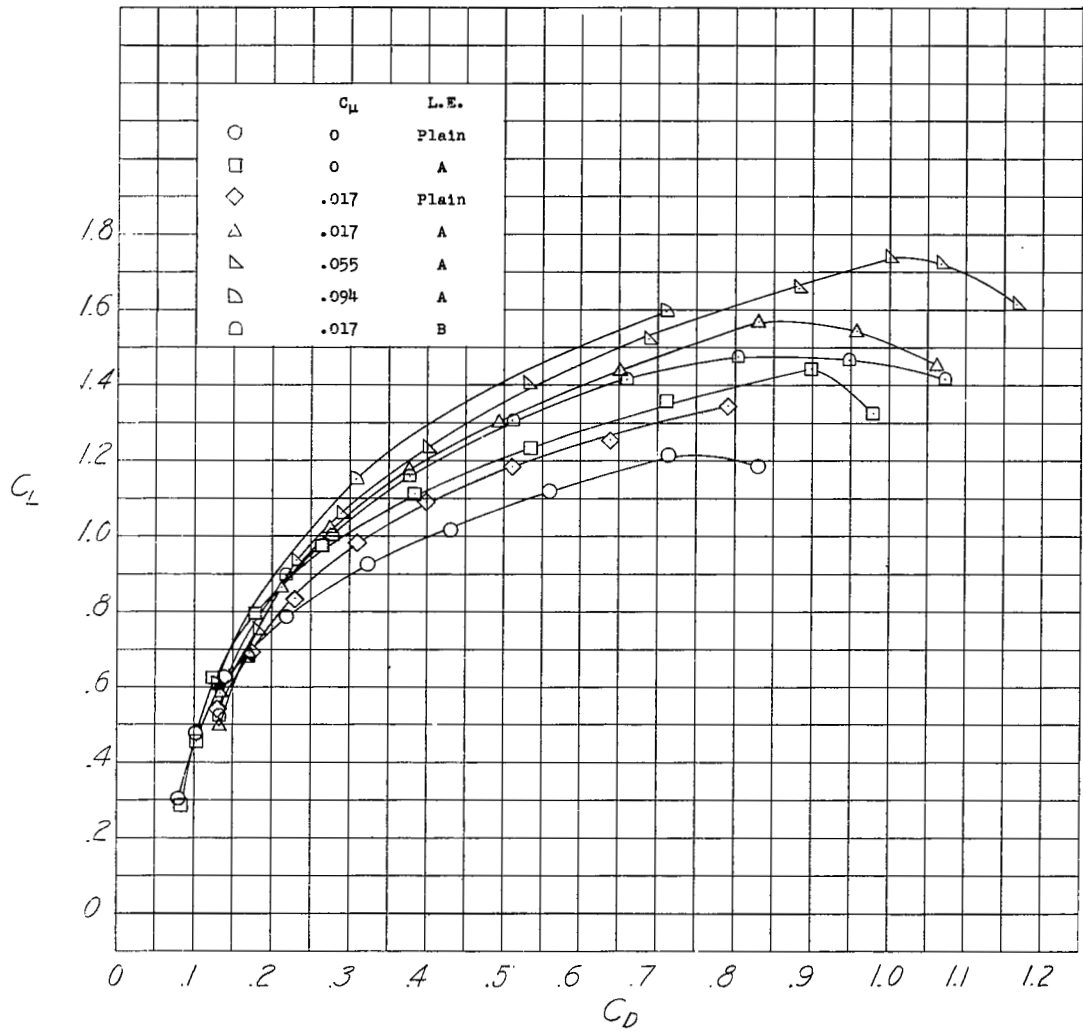
(b) Drag.

Figure 10.- Concluded.



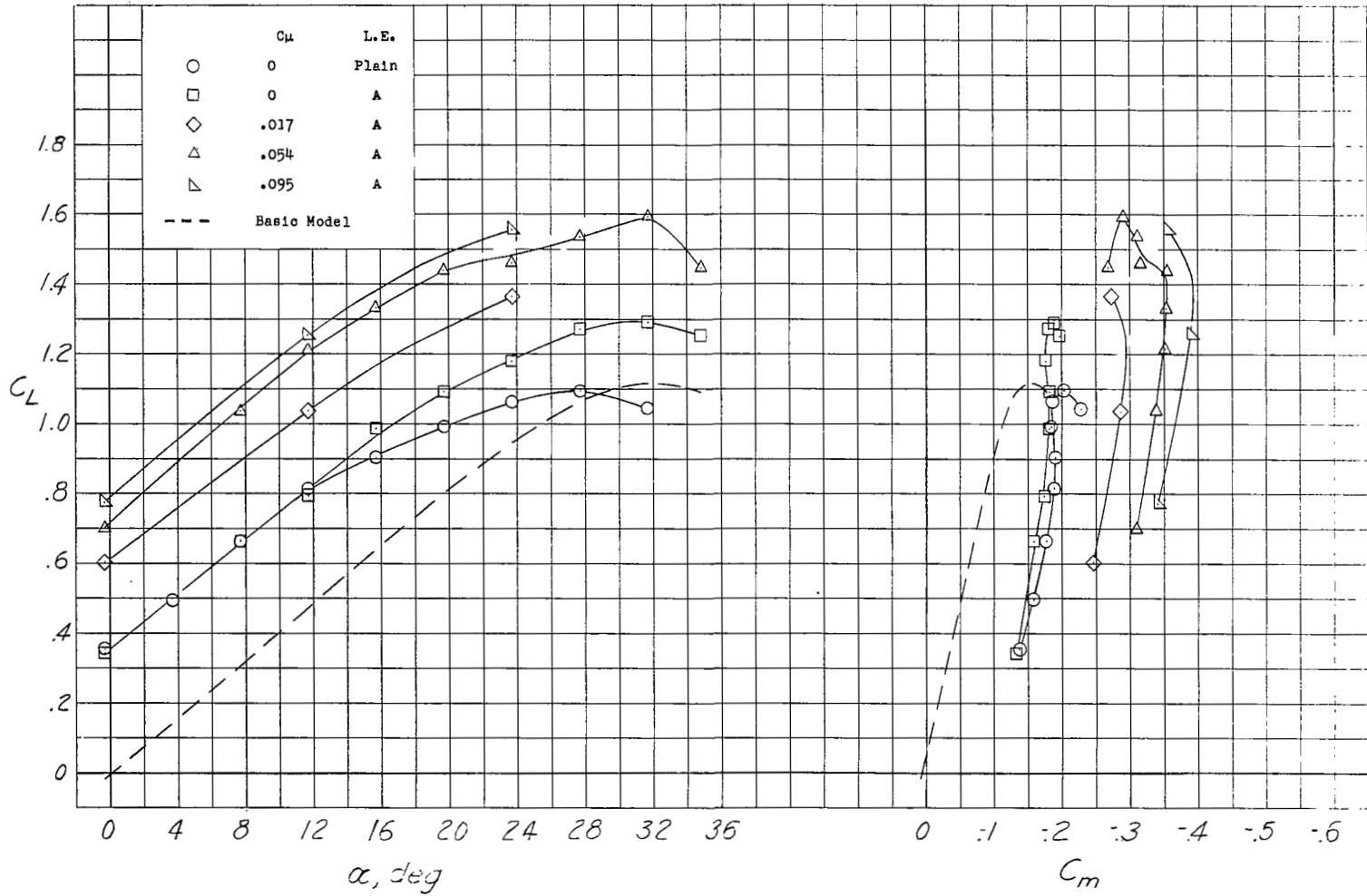
(a) Lift and pitching moment.

Figure 11.- Longitudinal characteristics of the model with semispan flaps deflected 45°. Tail off.



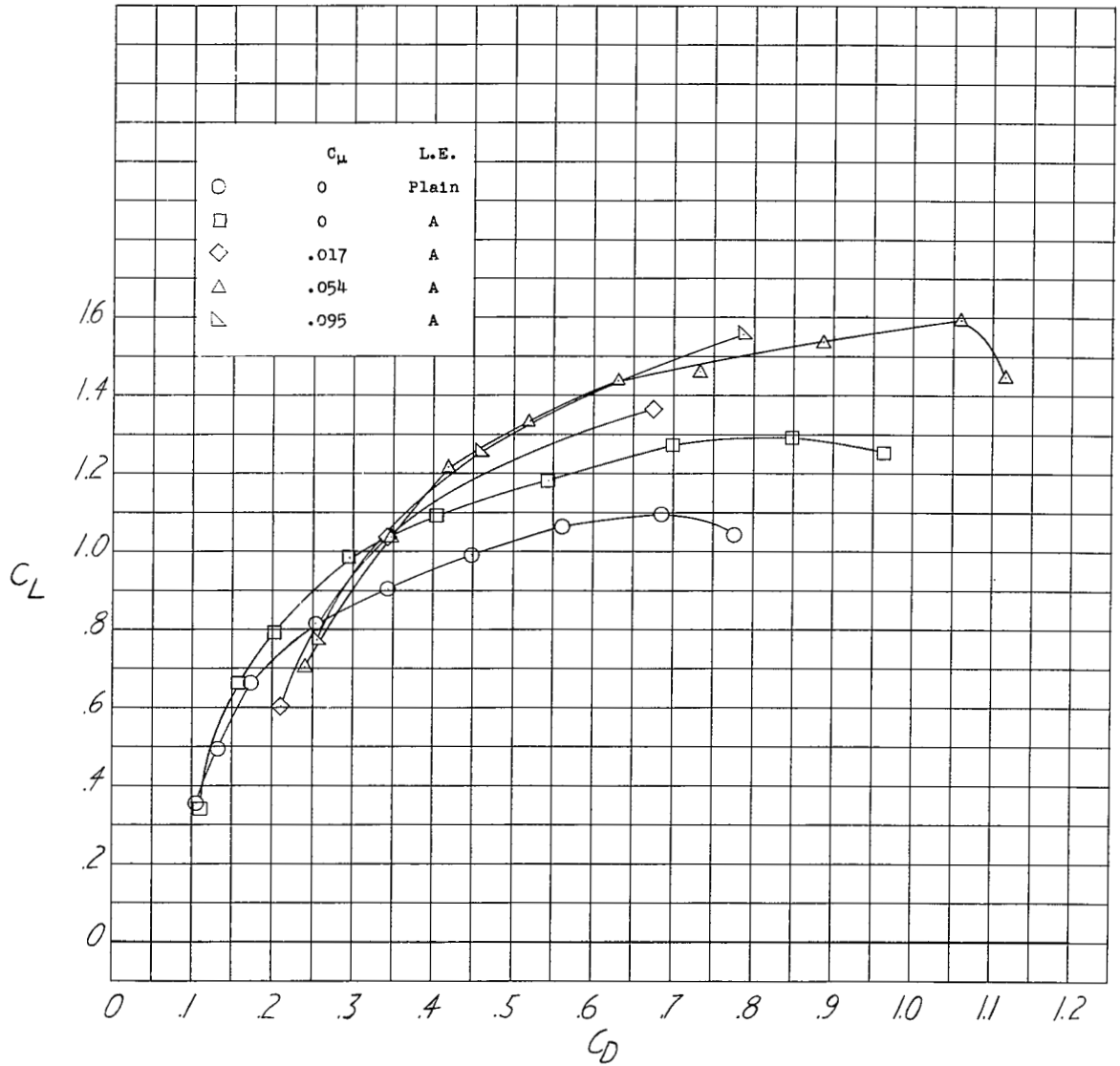
(b) Drag.

Figure 11.- Concluded.



(a) Lift and pitching moment.

Figure 12.- Longitudinal characteristics of the model with semispan flaps deflected 60°. Tail off.



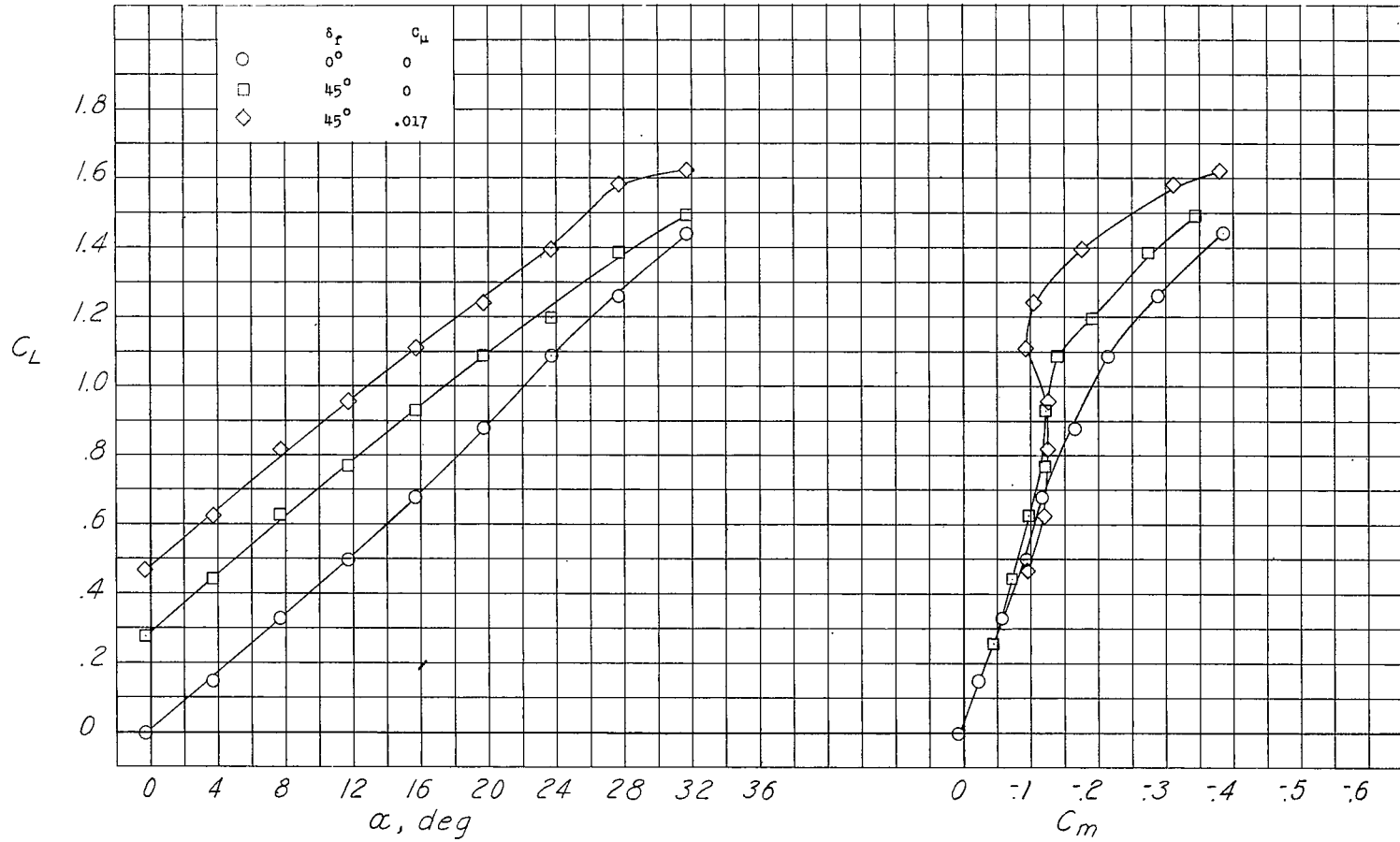
(b) Drag.

Figure 12.- Concluded.



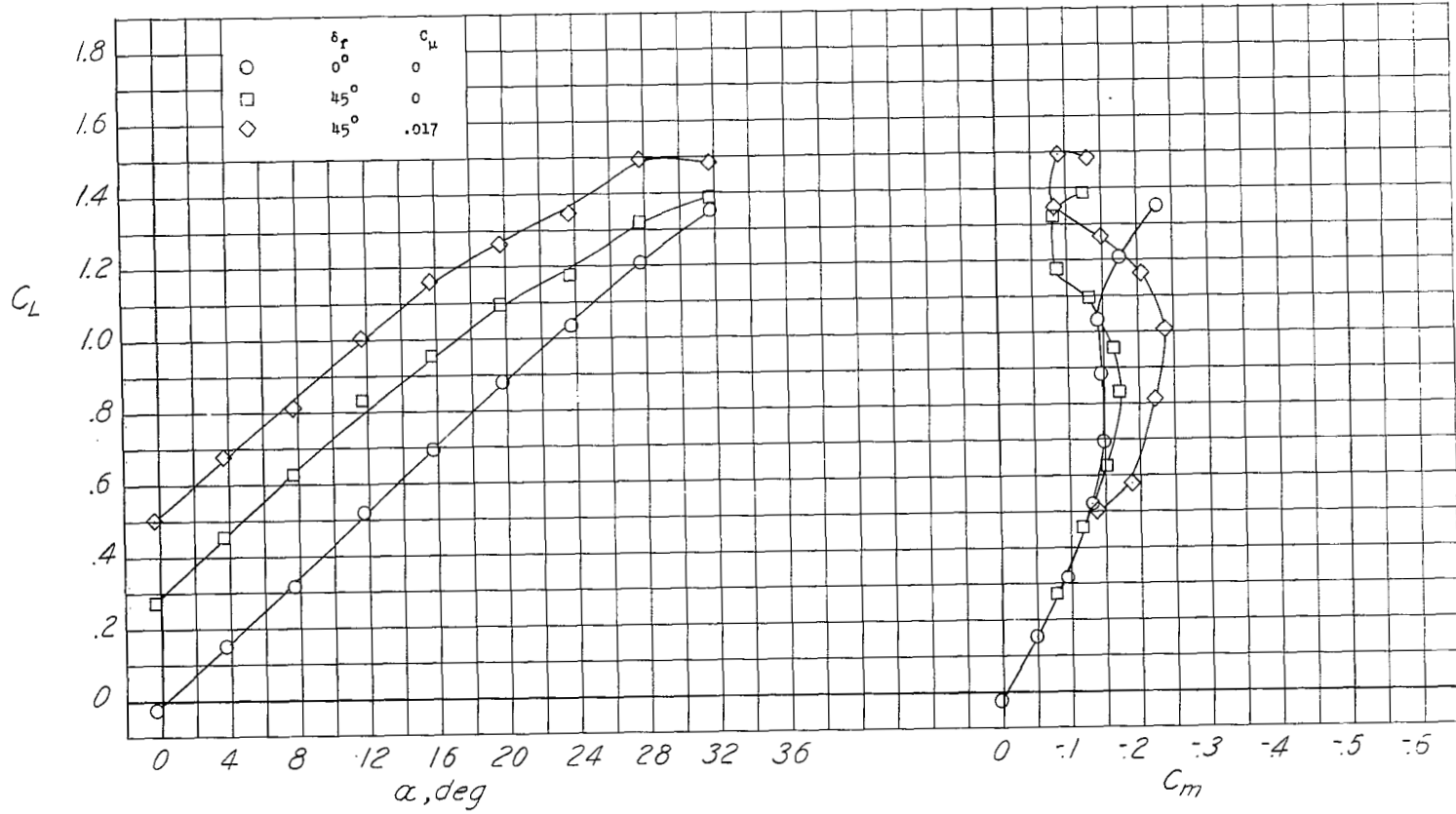
(a) $x/\bar{c} = 2.0$; $z/\bar{c} = -0.14$.

Figure 13.- Effect of semispan-flap deflection, blowing on semispan flaps, and tail location on the longitudinal stability of the delta-wing model with a 0.20S delta tail. Leading edge A.



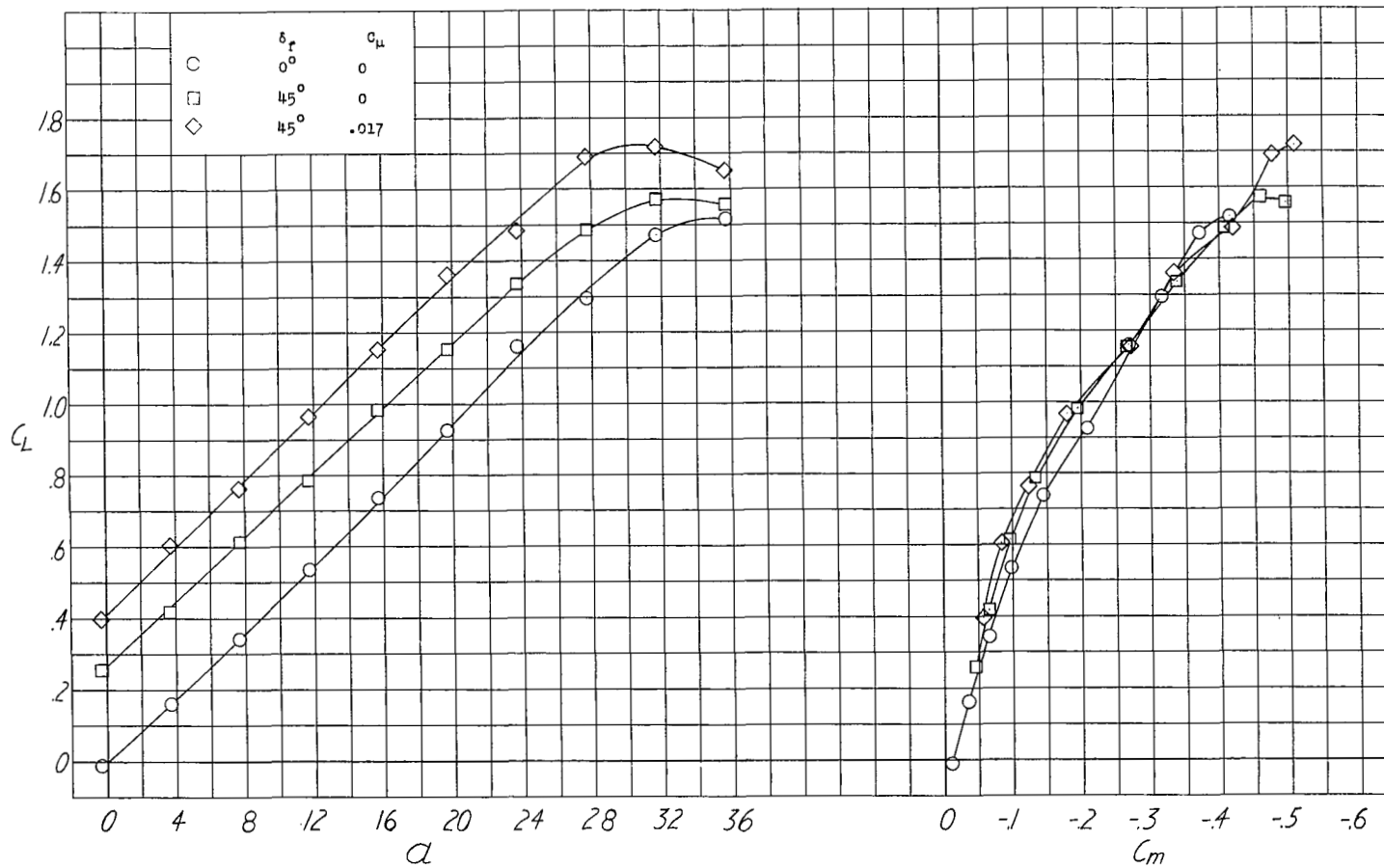
(b) $x/\bar{c} = 2.0$; $z/\bar{c} = 0.25$.

Figure 13.- Continued.



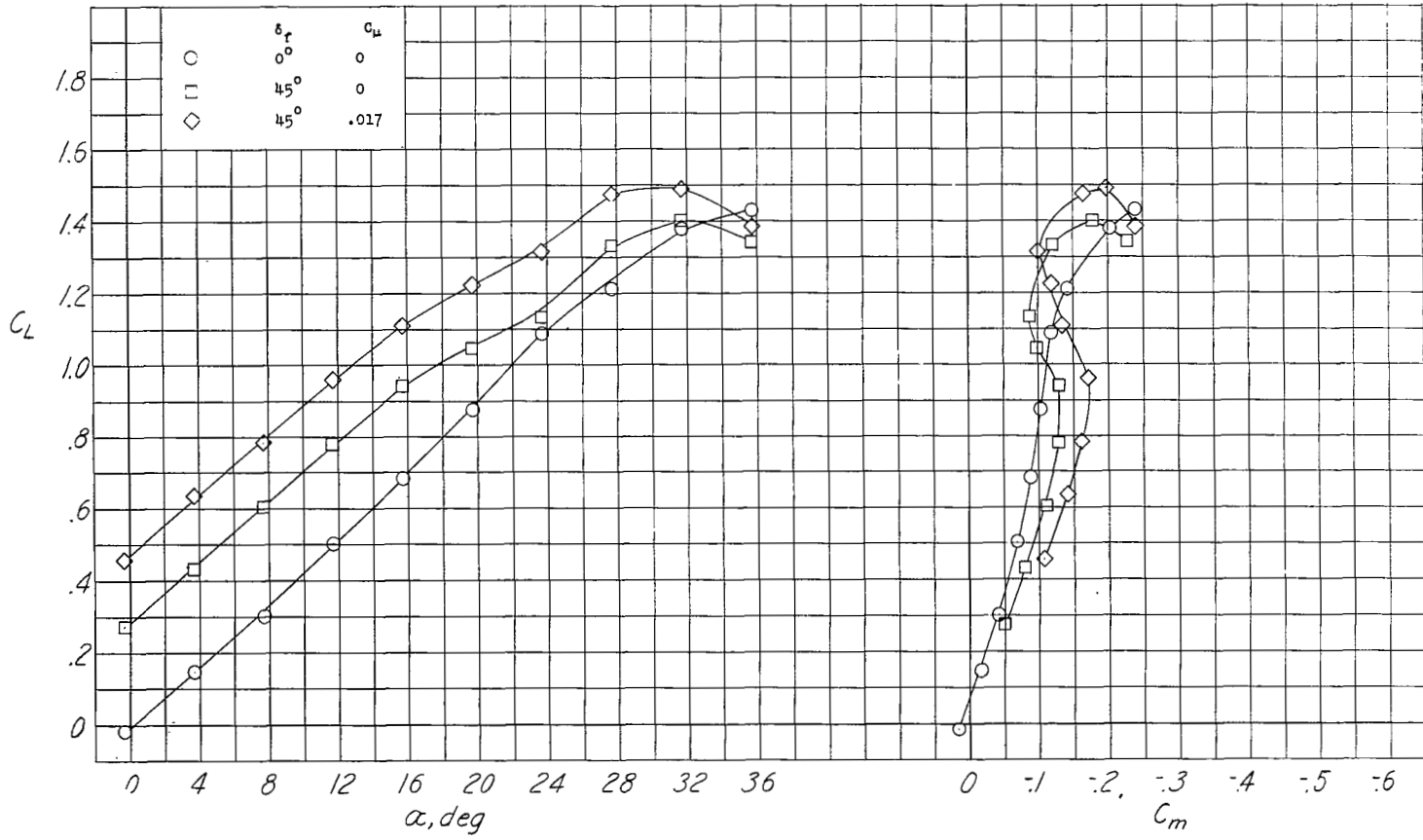
(c) $x/\bar{c} = 2.0$; $z/\bar{c} = 0.50$.

Figure 13.- Continued.



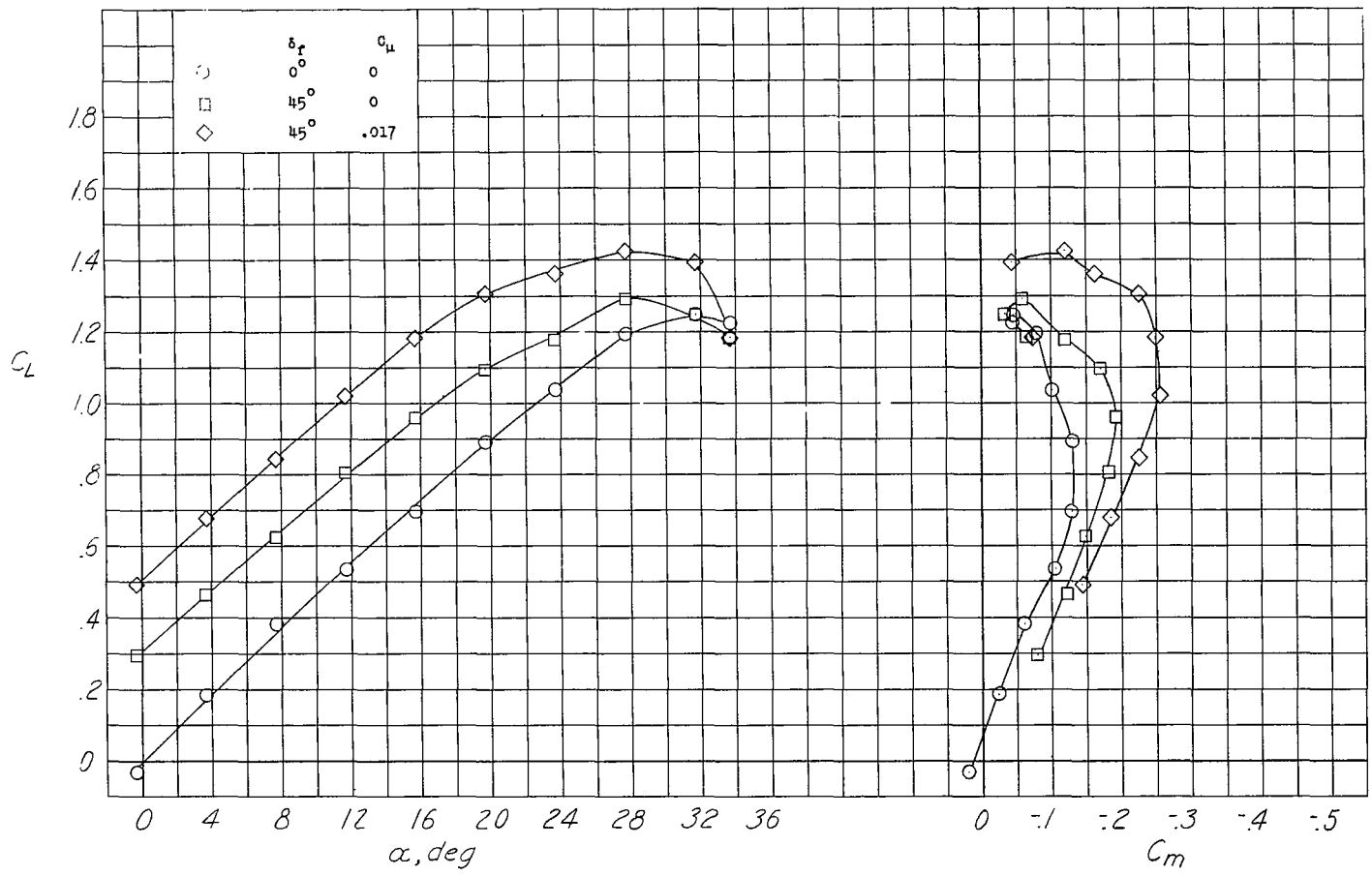
(a) $x/\bar{c} = 1.5$; $z/\bar{c} = -0.14$.

Figure 13.- Continued.



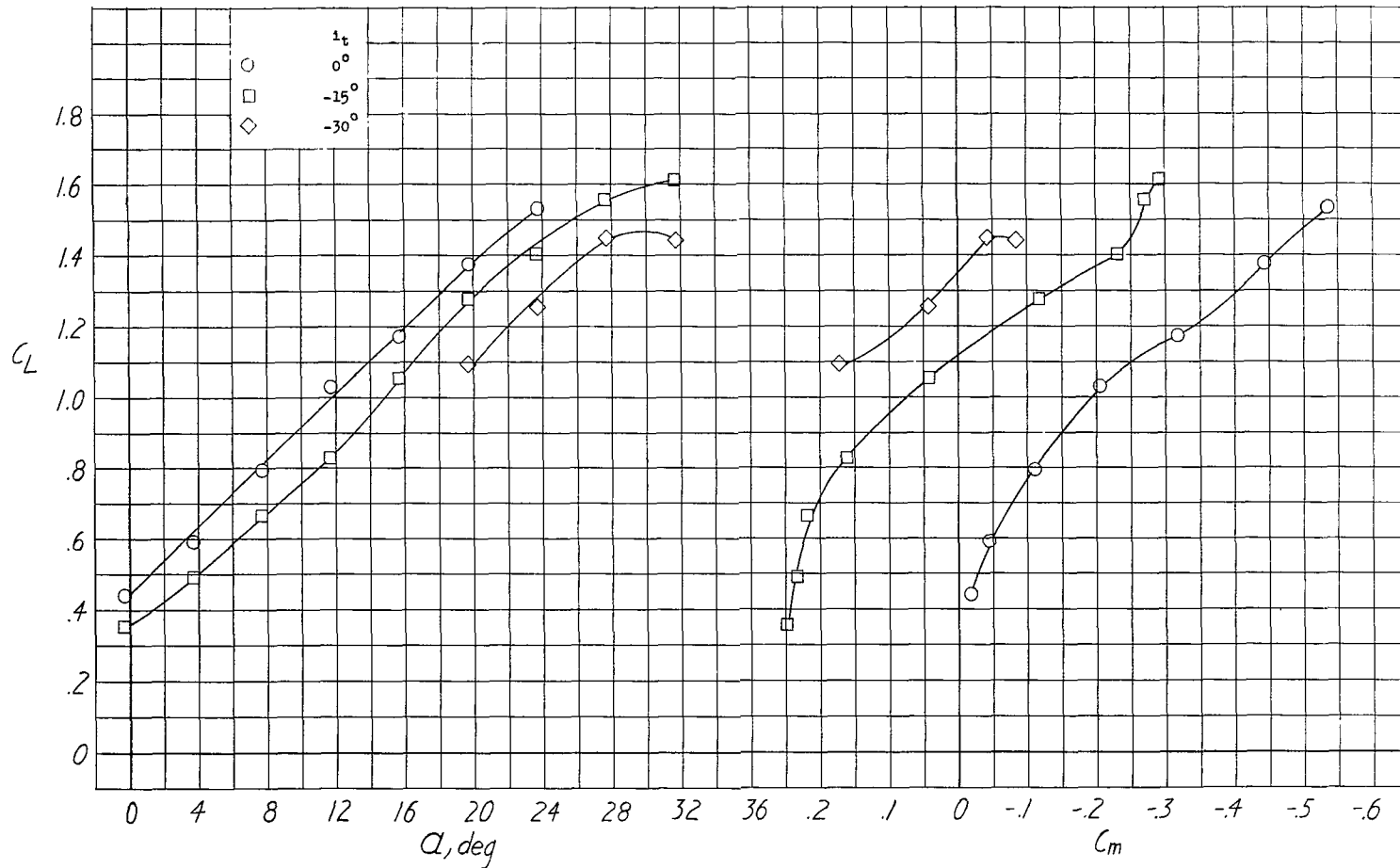
(e) $x/\bar{c} = 1.5$; $z/\bar{c} = 0.25$.

Figure 13.- Continued.



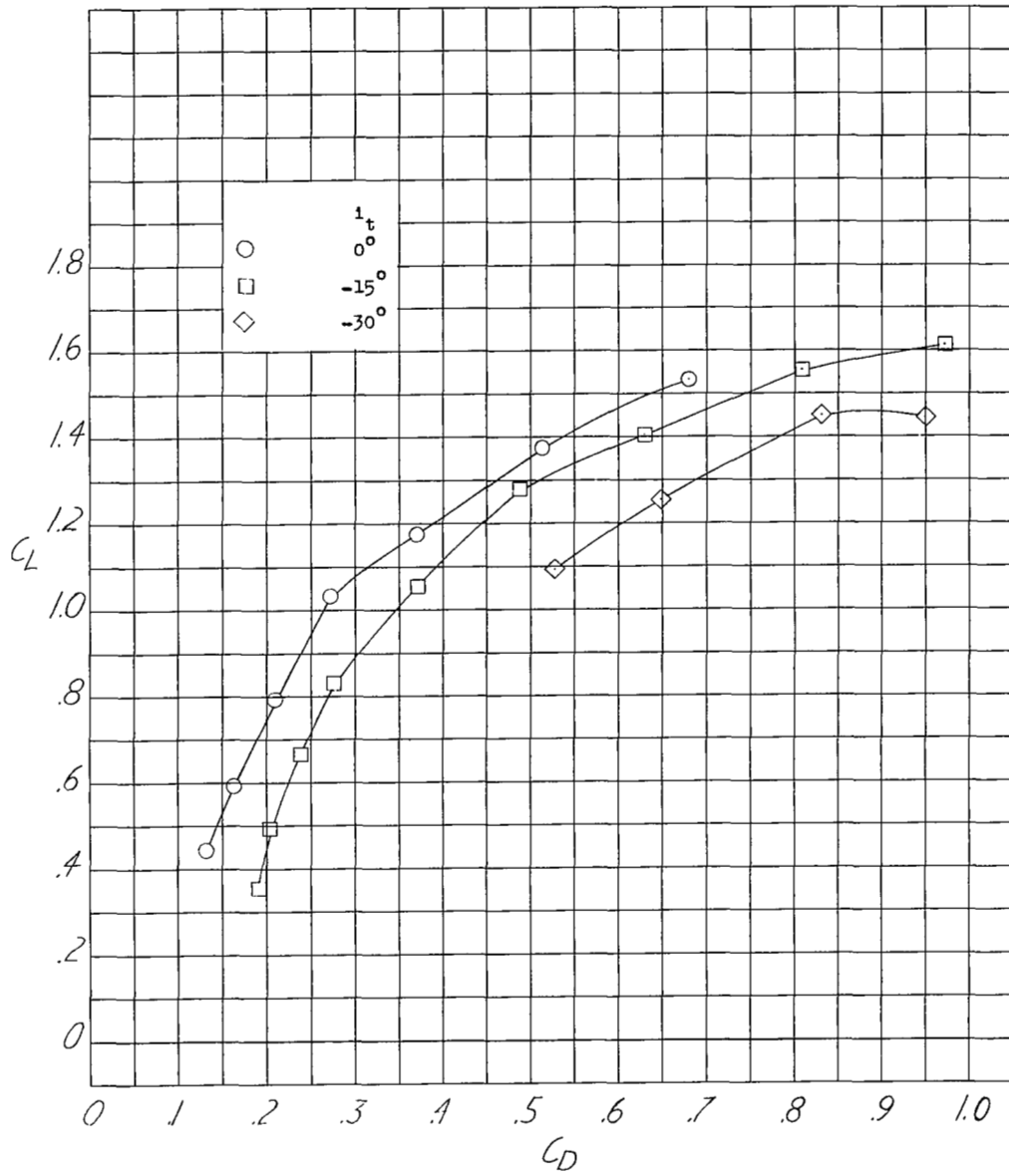
(f) $x/\bar{c} = 1.5$; $z/\bar{c} = 0.50$.

Figure 13.- Concluded.



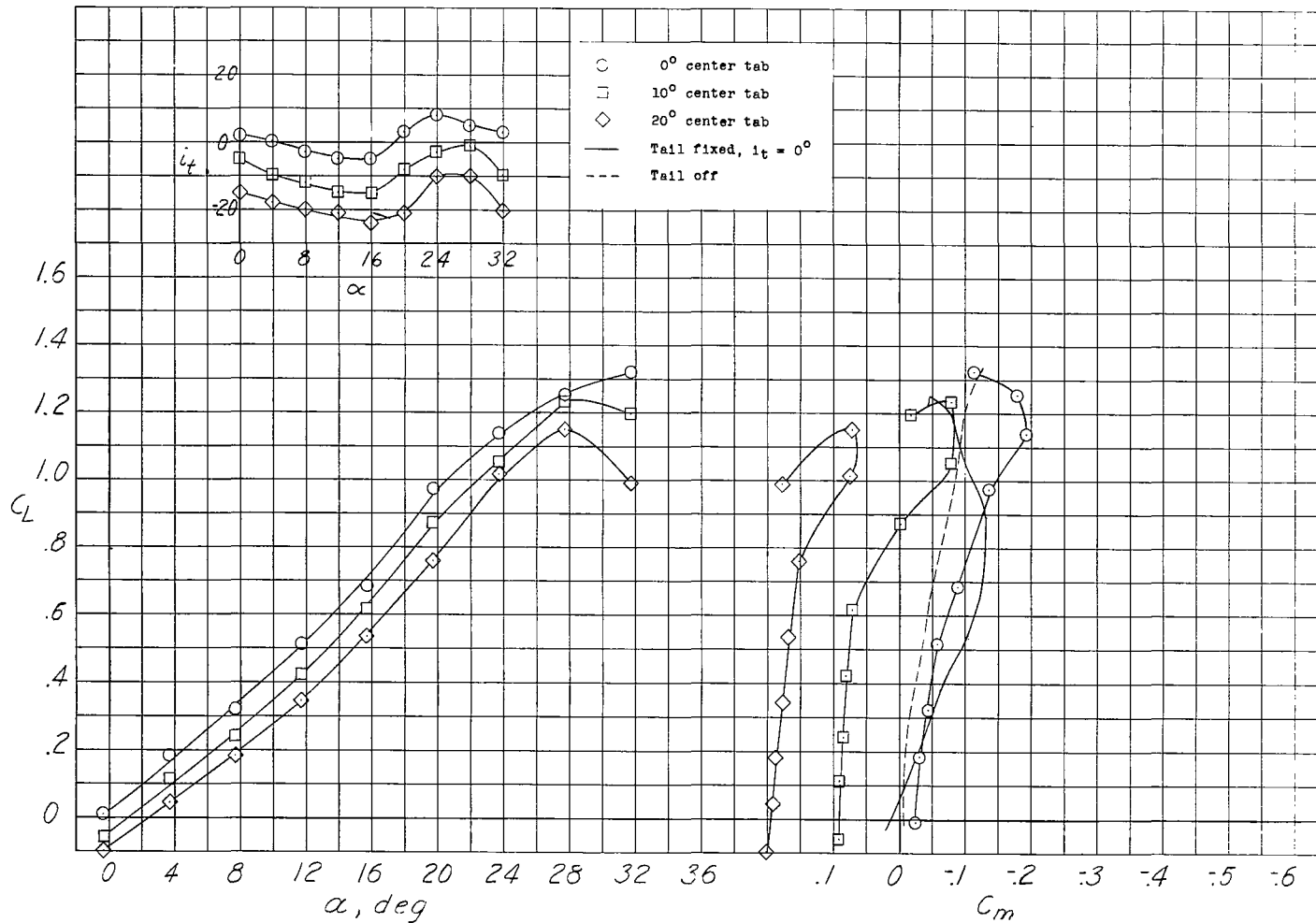
(a) Lift and pitching moment.

Figure 14.- Effect of horizontal-tail deflection on the longitudinal characteristics of the delta-wing model with blowing on semispan flaps. Leading edge A; $\delta_f = 45^\circ$; $C_\mu = 0.017$; $x/\bar{c} = 2.0$; $z/\bar{c} = -0.14$.



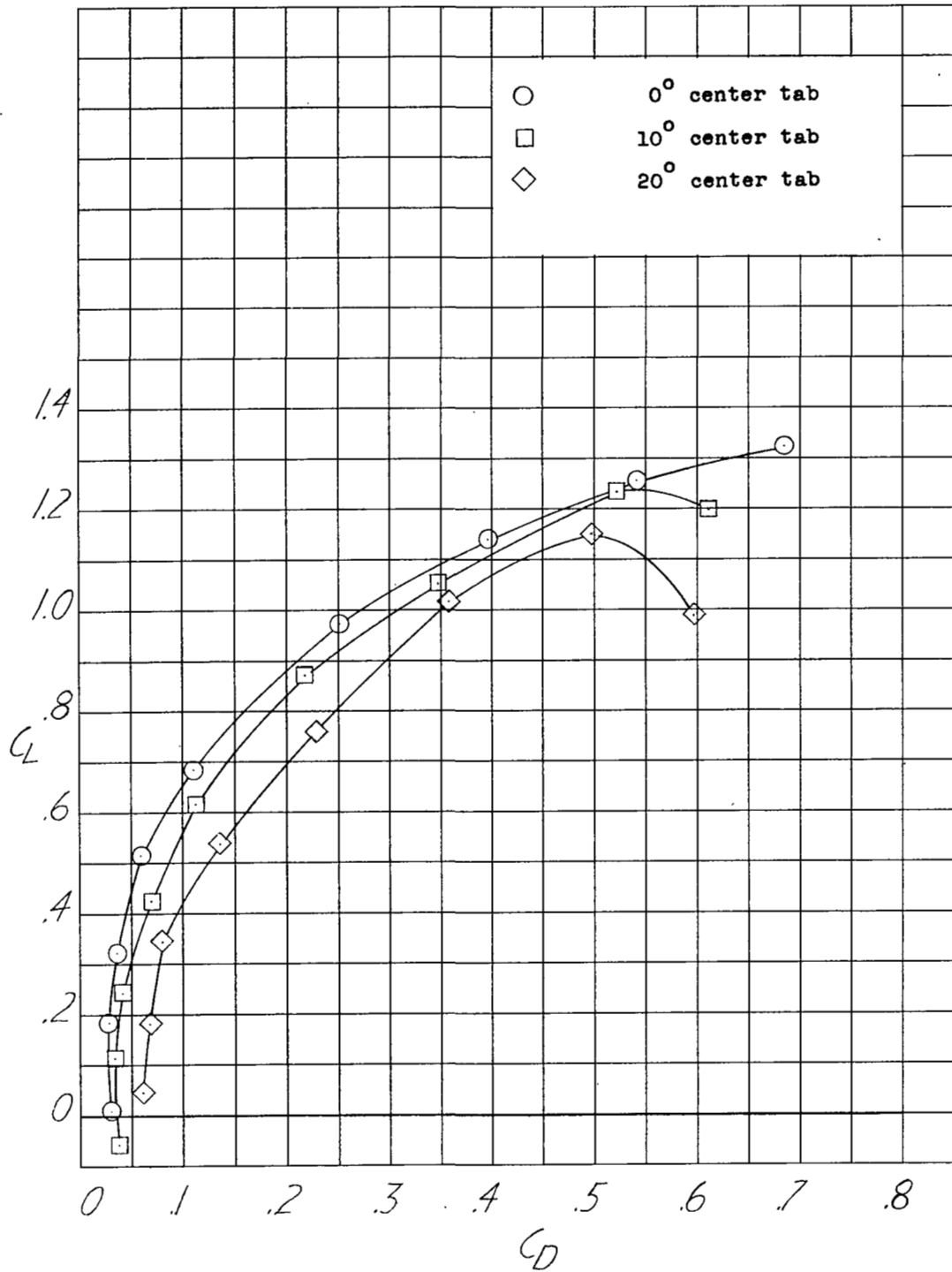
(b) Drag.

Figure 14.- Concluded.



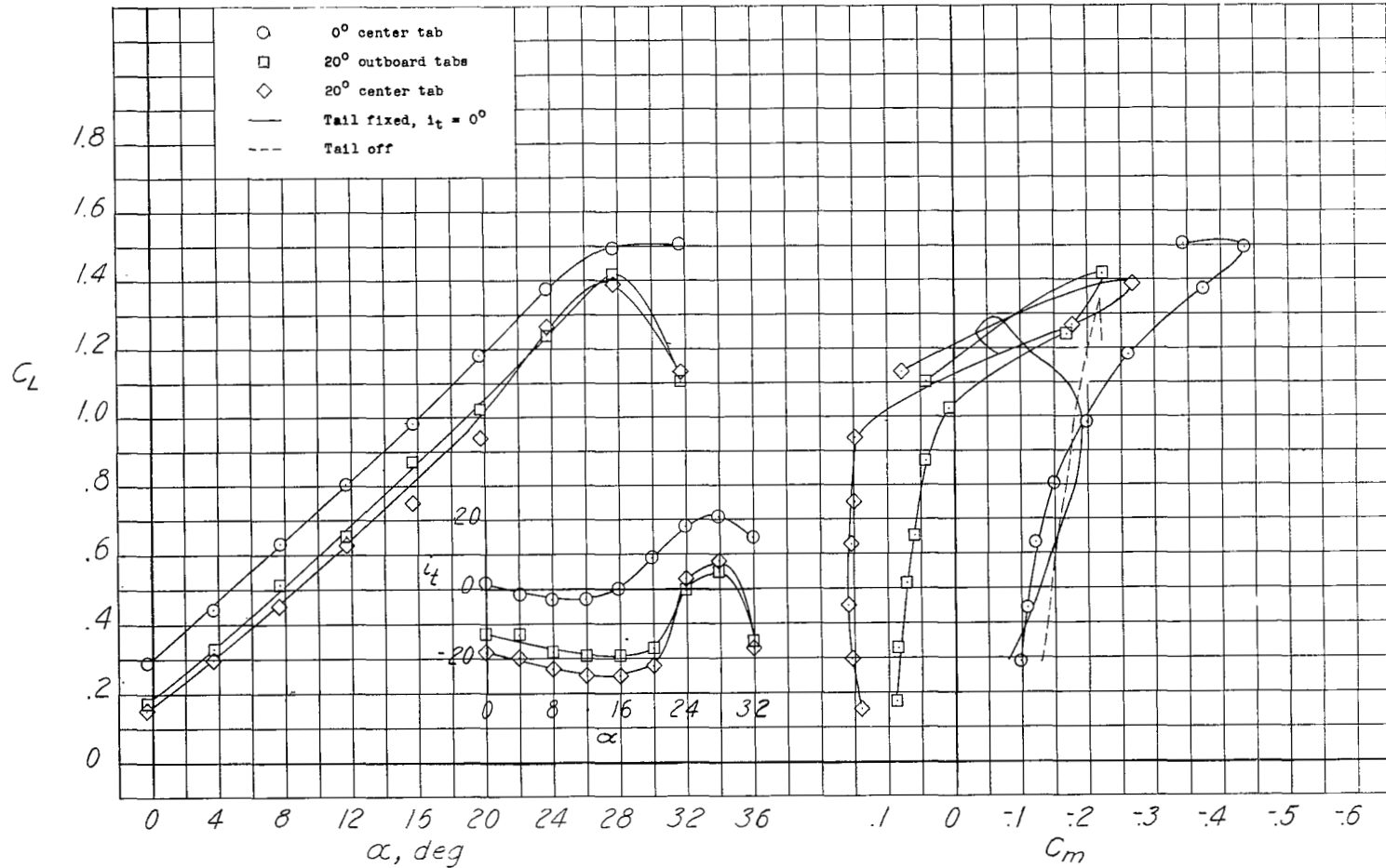
(a) Lift and pitching moment.

Figure 15.- Effect of free-floating delta tail on the longitudinal characteristics with the semi-span flaps neutral. Leading edge A; $C_{\mu} = 0$; $x/\bar{c} = 1.5$; $z/\bar{c} = 0.50$.



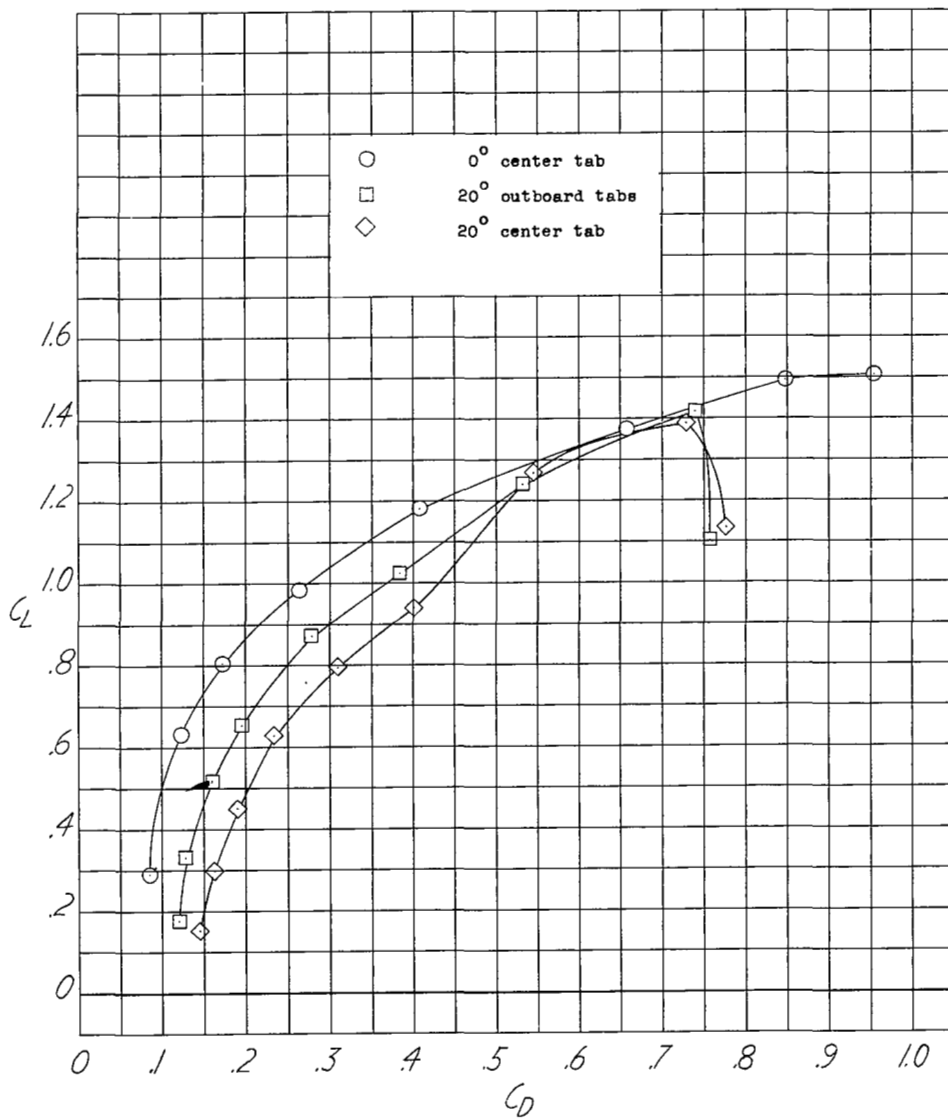
(b) Drag.

Figure 15.- Concluded.



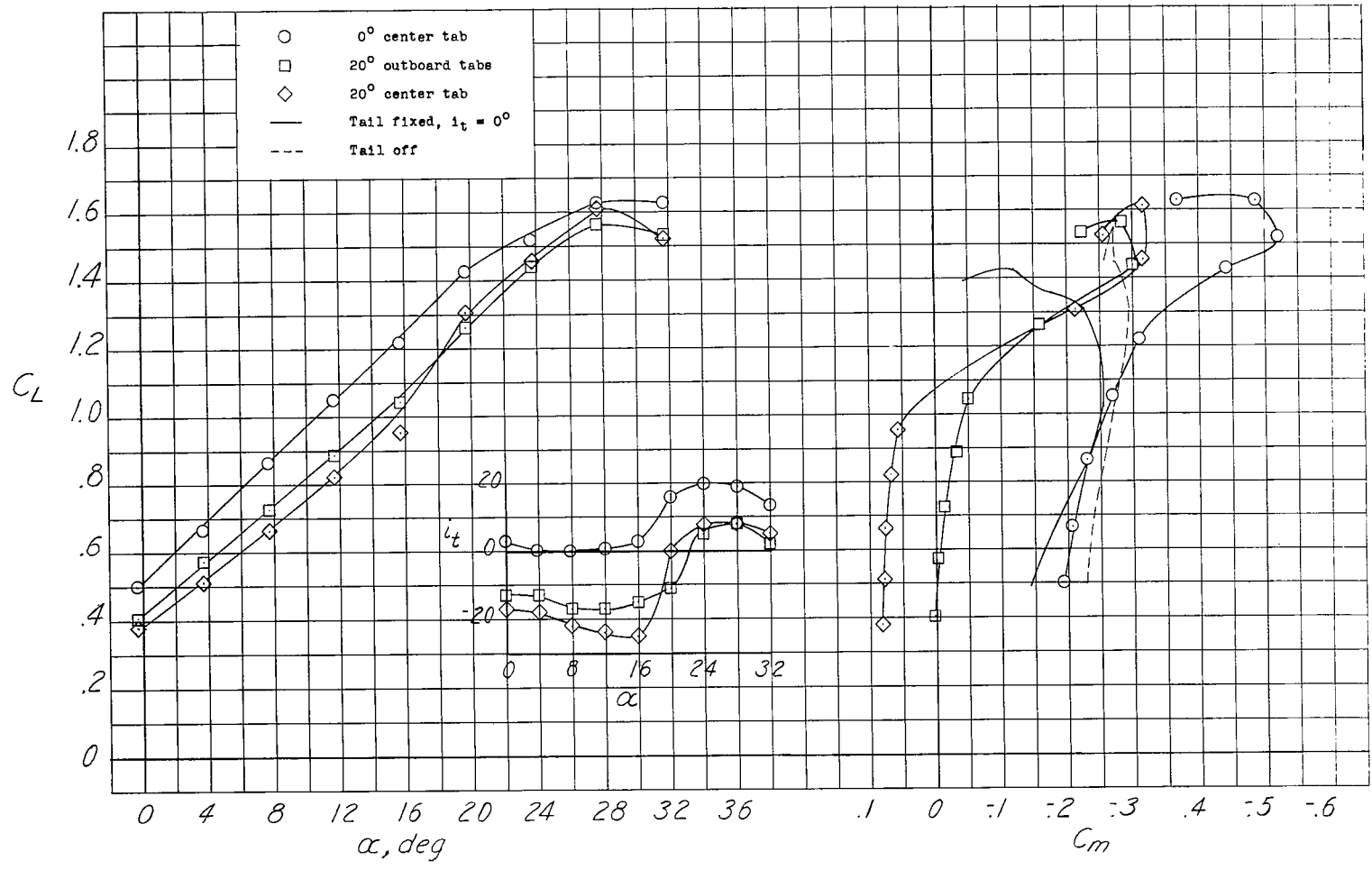
(a) Lift and pitching moment.

Figure 16.- Effect of free-floating delta tail on the longitudinal characteristics with the semi-span flaps deflected 45° . Leading edge A; $C_{\mu} = 0$; $x/\bar{c} = 1.5$; $z/\bar{c} = 0.50$.



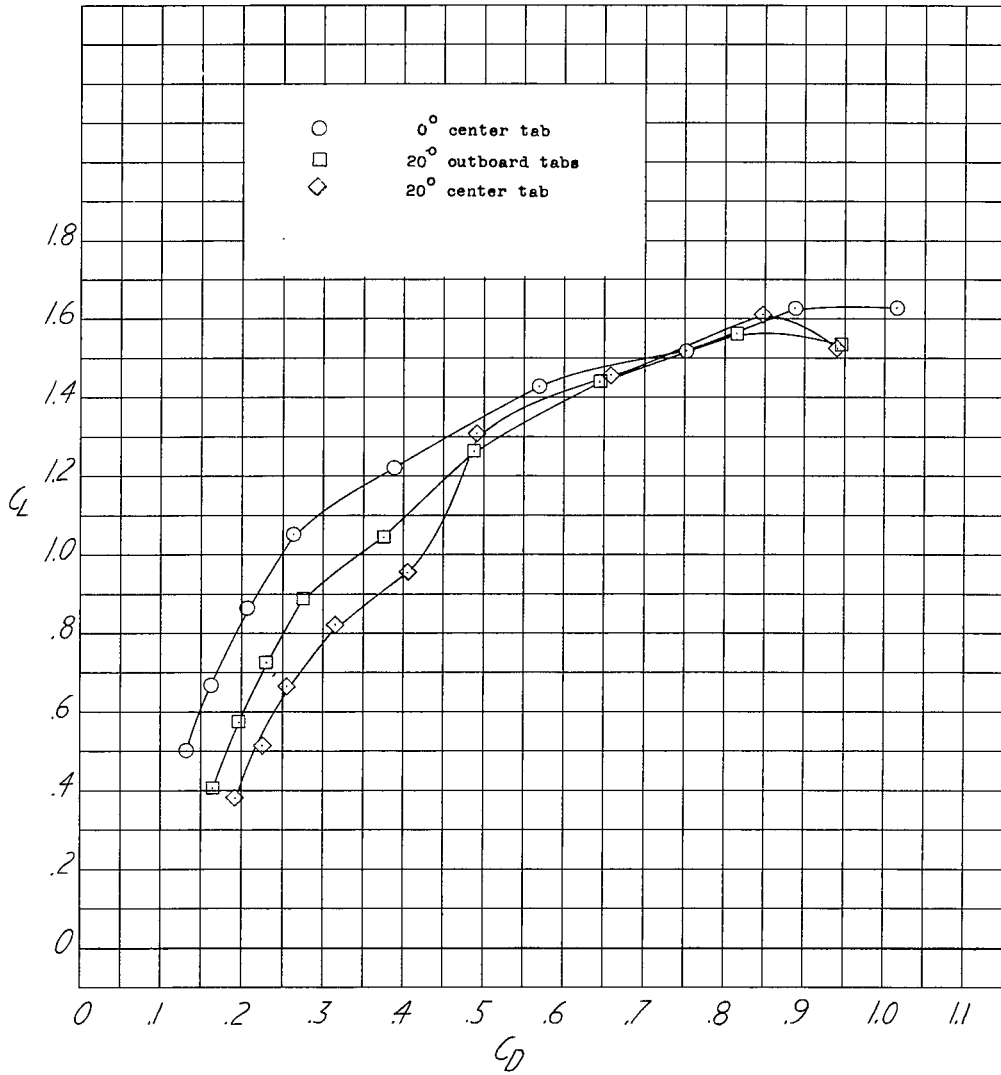
(b) Drag.

Figure 16.- Concluded.



(a) Lift and pitching moment.

Figure 17.- Effect of free-floating delta tail on the longitudinal characteristics with the semi-span flaps deflected 45° . Leading edge A; $C_{\mu} = 0.017$; $x/\bar{c} = 1.5$; $z/\bar{c} = 0.50$.



(b) Drag.

Figure 17.- Concluded.

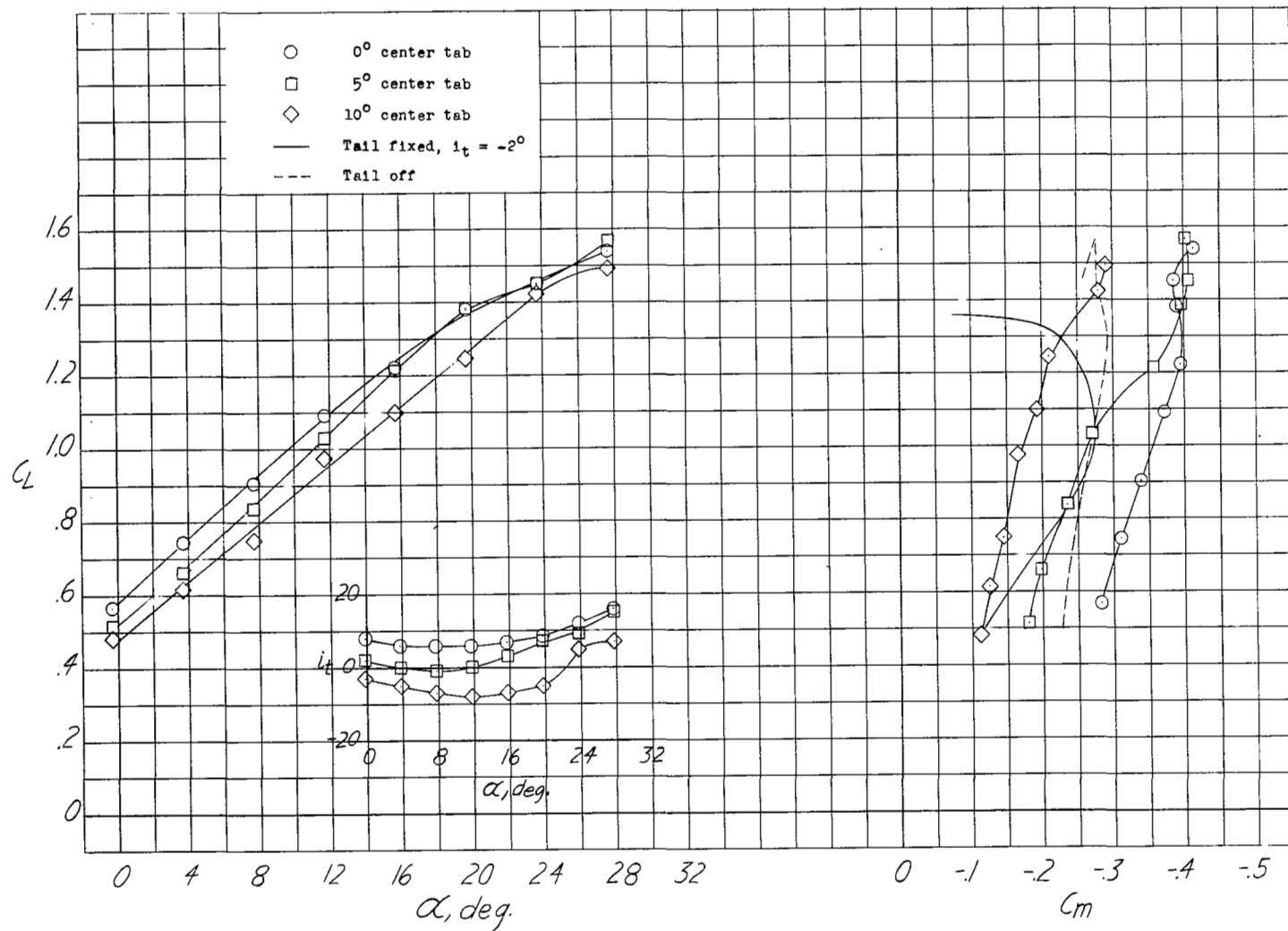


Figure 18.- Effect of free-floating unswept tail on the longitudinal characteristics with the semispan flaps deflected 45° . Leading edge B; $C_{\mu} = 0.017$; $x/\bar{c} = 1.5$; $z/\bar{c} = 0.50$.

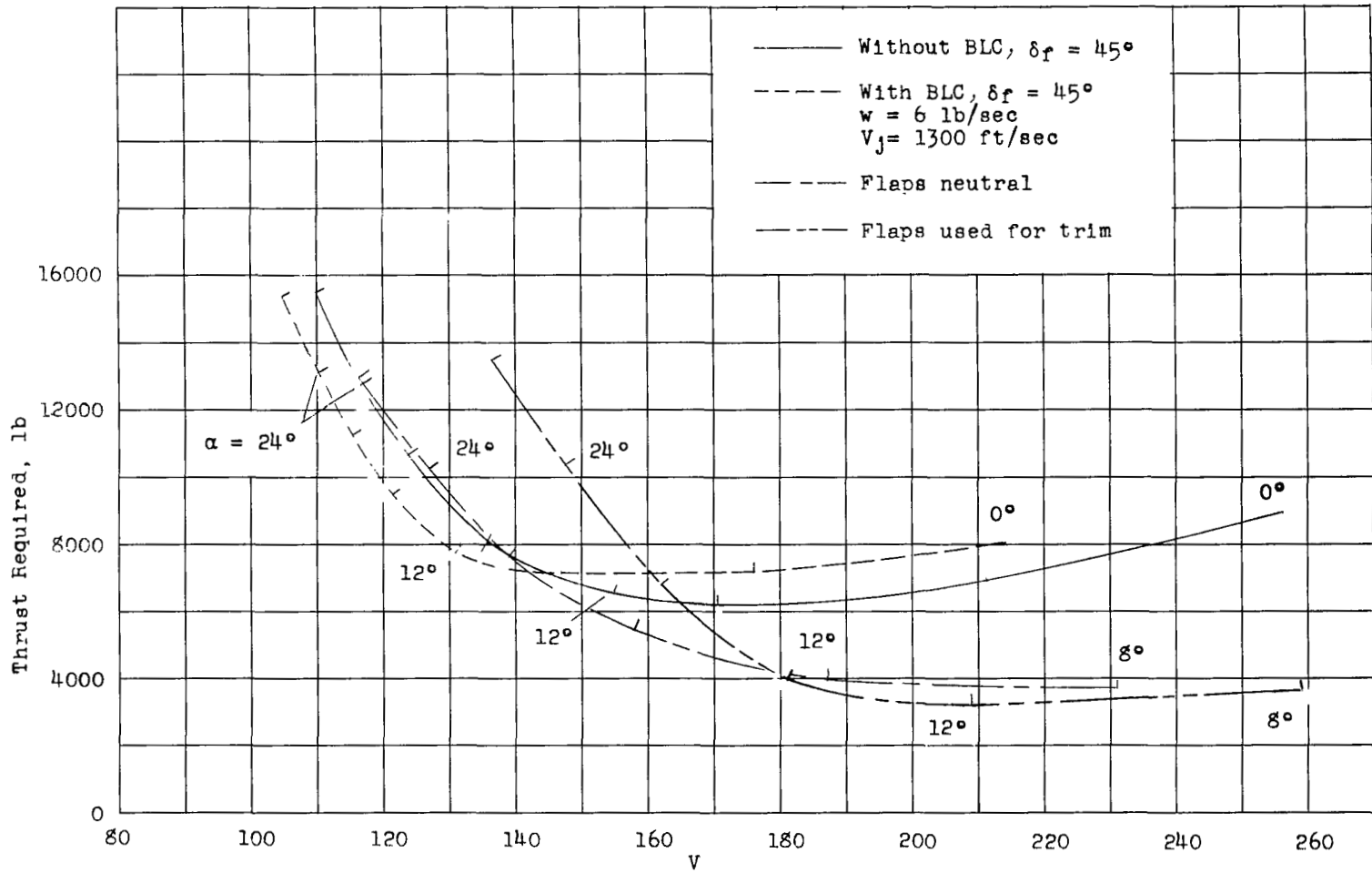


Figure 19.- Comparison of low-speed performance of a hypothetical delta-wing airplane.
 $W = 30,000 \text{ lb}$; $W/S = 60$; trimmed with dC_m/dC_L , with flaps neutral, reduced to -0.075 ;
 $x/\bar{c} = 2.0$; $z/\bar{c} = -0.14$; leading edge A.

NASA Technical Library



3 1176 01438 1074

